T H E U N I V E R S I T Y O F T U L S A

THE GRADUATE SCHOOL

TRANSIENT MODELING OF PLUNGER LIFT FOR GAS WELL LIQUID UNLOADING

by
Qingqi Zhao

A thesis submitted in partial fulfillment of

the requirements for the degree of Master of Science

in the Discipline of Petroleum Engineering

The Graduate School

The University of Tulsa

2020

T H E U N I V E R S I T Y O F T U L S A

THE GRADUATE SCHOOL

TRANSIENT MODELING OF PLUNGER LIFT FOR GAS WELL LIQUID UNLOADING

by
Qingqi Zhao

A THESIS

APPROVED FOR THE DISCIPLINE OF

PETROLEUM ENGINEERING

By Thesis Committee

Hong-Quan Zhang, Chair
Ovadia Shoham
Baojun Song
Haiwen Zhu

COPYRIGHT STATEMENT

Copyright © 2020 by Qingqi Zhao

All rights reserved. No part of this publication may be reproduced, stored in a retrieval system, or transmitted, in any form or by any means (electronic, mechanical, photocopying, recording, or otherwise) without the prior written permission of the author.

ABSTRACT

Qingqi Zhao (Master of Science in Petroleum Engineering)

Transient Modeling of Plunger Lift for Gas Well Liquid Unloading

Directed by Dr. Hong-Quan (Holden) Zhang

92 pp, Chapter 5: Conclusions and Recommendations

(318 words)

A natural gas production well is commonly accompanied by liquid condensate. As gas wells mature, production rate and bottom-hole pressure decrease, resulting in liquid loading since the gas cannot carry the liquids to the surface. As a result, the liquids are accumulated at the bottom hole, which increases hydrostatic pressure, reduces gas production, and eventually kills the well. As an economical artificial lift method, plunger lift can be used to remove liquids from high gas/liquid ratio (GLR) wells. Therefore, the well bottom-hole pressure can be maintained low and gas can be produced at a high flow rate. However, the transient flow behavior of plunger lift wells is not well understood. In this study, a transient mechanistic model is developed to simulate the entire dynamic process of plunger lift cyclically paced by a surface control valve.

Starting with the Gasbarri and Wiggins (2001) dynamic plunger lift model, four stages in the cyclic movement of a plunger can be identified and calculated by a set of specific governing equations for plunger upstroke, gas blowout, plunger fall-down, and pressure buildup. Considering

the gas flows with a plunger moving in the tubing, the model can give the instant velocities during the rising and falling of the plunger. Vogel's Inflow Performance Relationship (IPR) (Vogel, 1968) is used as the reservoir model to obtain the fluid flow from the reservoir to the well-bore. The plunger model is able to capture all the essential features of the plunger cycle: the plunger velocity/acceleration, pressure versus time, production rate versus time, etc. Compared with the previous models, the equations of the rising speed and the falling speed of the plunger are improved. Hydrocarbon mixture in the gas well is also considered in the modified model which provides more accurate and reasonable predictions of tubing and casing pressure. Future improvement of the plunger lift model can be accomplished by adding liquid leakage around the plunger, and liquid slug discharge dynamics.

ACKNOWLEDGEMENTS

First of all, I am very grateful for the valuable suggestions, support, and guidance of my academic advisor, Dr. Hong-Quan Zhang. I will always remember the first call with Dr. Zhang. It was the beginning of my story in Tulsa. Thank you for giving me the opportunity to study at TU. It will be a very good memory in my life. I have learned so much and had a lot of help from Dr. Zhang. I deeply admire his rigorous study and tireless attitude towards scientific research. I am also interested in Dr. Zhang's research on atmospheric science and the Earth's water cycle. I am deeply impressed with Dr. Zhang's unique analysis and bold conjecture.

I would like to thank Dr. Jianjun Zhu, who used to be a post-doctoral research associate at TUALP and is now working at China University of Petroleum (Beijing). With his help and guidance, I began to learn how to do research. Dr. Jianjun Zhu taught me how to use OLGA and suggested that me I learn the Python programming language. Special thanks are given to Dr. Haiwen Zhu, a post-doctoral research associate at TUALP. He helped me prepare ABM presentations and improve technical writing skills. Although he is currently stranded in China by the ongoing coronavirus pandemic, Dr. Haiwen Zhu has been keeping in touch with me and helping me conduct my research. With his great assistance, I can complete my thesis.

I give special thanks to Ms. Donna Trankley for her administrative work. I am very grateful for my TUALP team members: Yi Shi, Guangqiang Cao, Jianlin Peng, Zimo Lin, Chengcheng Luo, Zhengjing Shen, Muhammad Rasyid Ridlah and Nursultan Bakyt, for their help, support, and friendship. I appreciate Dr. Ovadia Shoham, and Dr. Baojun Song for being on my thesis committee.

My deepest gratitude goes to my family for their support and love throughout my life: my parents Yuli Zhao and Xiaowen Liu. No matter how difficult it is, they always give me the best. Even on the other side of the Earth, they care about me all the time. I know you have sacrificed so much to support me. Dad and Mom, I love you forever.

TABLE OF CONTENTS

LIST OF FIGURES

LIST OF TABLE

INTRODUCTION

As an intermittent artificial lifting method, plunger lift is commonly used to remove liquids from gas wells or relatively low production rates but high GOR oil wells. Different from other artificial lift methods, the plunger lift is operated by the energy from the well to unload liquid. The liquid loading occurs near the well bottom due to the accumulation of liquid (Fan et al., 2018), which adds a considerable back pressure to the reservoir and further reduces the gas production rates (Hashmi et al., 2018; Zhang et al., 2018; Wang et al., 2019). Under this condition, the produced liquids will continuously accumulate in the wellbore, which reduces the production and the well-producing life span.

A plunger cycle starts in the shut-in period when the control valve at the surface closes and the plunger drops from the surface to the bottom of the well. In the upward period, the well pressure is built by the accumulated gas in the annulus and the near-wellbore region of the reservoir. Thereafter, the plunger and liquid slug are lifted to the surface against surface-line pressure and friction. The gas from both annulus and the near-wellbore reservoir will expand into tubing to provide enough energy to lift the plunger to the surface. In this period, the surface production rate and tubing pressure drop sharply due to the rapidly reduced differential pressure between casing and tubing.

After the plunger arrives at the surface and the liquid is unloaded, the gas production rate increased sharply since the well begins to produce free of liquids. As the production rate and gas velocity drop below the critical values, liquid is accumulated at the tubing bottom again. Then, the

well is shut-in and the plunger falls back to the bottom. Thereafter, a new cycle starts and the lift cycle repeats one after another.

In general, plungers are installed in high gas-liquid ratio (GLR) oil wells or liquids loaded gas wells. The GLR and gas rate need to be high enough to provide energy in order to lift liquids from the bottom hole. Compared with other artificial lift methods such as rod pump and ESP, the main advantages of plunger lifting are the relatively lower investment and operation cost. The disadvantage of the plunger lifting system is that the lifting process is complex, and the optimization and troubleshooting of the lifting method are lack of understanding. In order to apply the optimization algorithm, an accurate mechanistic model of the transient plunger lifting process must be developed.

Several static models have been proposed and are widely used in the design because of its simplicity. The dynamic model that describes the circulation phenomenon of plunger lifting is also widely studied recently. The existing models are still insufficient due to oversimplification or individual assumptions. In this study, a new model will be developed considering changes of plunger rising and failing velocities, as well as combination with compositional model and black-oil model. The new plunger lift model will be compared with the simulation results of OLGA, a widely used transient commercial software.

CHAPTER 1

LITERATURE REVIEW

Artificial lift production is a method of artificially adding energy to the fluid and lifting it from the well bottom to the wellhead. With the increase of the total amount of gas (and liquid) produced, the reservoir pressure decreases and the water cut (WC) of the well increases. As a result, the self-flow ability of the gas well is weakened gradually. The artificial lifting method (also known as mechanical oil extraction) is the main way to increase production especially in the late stage of gas and oil field exploitation. The methods of lifting crude oil from the bottom of the well to the surface by artificial lift can be divided into two groups: gas lift methods and pumping methods.

The pumping methods mainly use can be further divided as rod pump and non-rod pump. Sucker rod pumping is a kind of artificial lifting oil production method that the pumping unit drives the piston to move up and down by the sucker rod in the well to pump the oil to the ground. This method accounts for 80% - 90% of all the wells in the world. Non-rod pump production refers to the underground pump driven by motor or high-pressure liquid instead of using sucker rod to transfer power, including electric submersible pump, screw pump, jet pump, and hydraulic piston pump.

For the gas lift method application, the gravitational term is dominant and the bottom hole flowing pressure is not high enough to lift the crude oil from the well bottom to the surface. Therefore, it is necessary to inject the gas into the bottom of the well artificially and lift the crude

oil out of the ground. The lifting principle is similar to that of a natural flowing well. High-pressure gas is injected into the annulus of the casing and then enters tubing through gas lift valves. As a result, the density of the mixture in the wellbore is reduced until it can be discharged out of the wellhead. At the same time, the volume of injected high-pressure gas increases gradually when it rises along the wellbore, and the carrying ability of the expanded gas also increases. Gas lift is suitable for oil wells with strong liquid supply capacity and high formation permeability, including but not limited to offshore oil production, deep well, deviated well, sand well, and gas and oil wells with corrosive components that are not suitable for other artificial lift methods. The advantages of gas lift production include simple wellhead and downhole equipment requirements, and convenient management and adjustment; the disadvantages are complex surface equipment system requirement, large investment, and low utilization of gas energy.

For gas well with limited liquid production, gas lift and pump lift method are no longer the appropriate options, and plunger lift is commonly the choice. Plunger lift is a reciprocating piston pumping method with high efficiency and flexibility. It can be used in vertical wells, inclined wells, and cluster wells. The system can effectively remove the bottom hole liquid accumulation, reduce the back pressure on the production layer and prevent water flooding, and extend the life of natural gas wells. Among the many liquid removal technologies, plunger lift is a simple, reliable and economical remedy for liquid-filled wells. As shown in Figure 1.1, a typical plunger lift system mainly comprises piston/plunger, surface control valve, catcher, lubricator/shock spring, bumper spring, plunger sensor, etc. A plunger lift system relies directly on the natural buildup of pressure in a shut-in gas well by the produced gas. The plunger lift cycle starts when the plunger is launched from the top of the bottom-hole bumper spring or when it is released from the surface lubricator. When the surface valve opens, the plunger travels from the bottom-hole bumper spring to the

surface. When the well is shut-in, the plunger falls to the bottom-hole bumper spring through the tubing. A motor valve is controlled at the surface and the differential pressure built during the well shut-in period forces the plunger to move up and lift the liquid to the surface. An arrival sensor recognizes and records plunger arrivals, plunger speeds, valve counts, and sets the controller to on, off or sales mode.

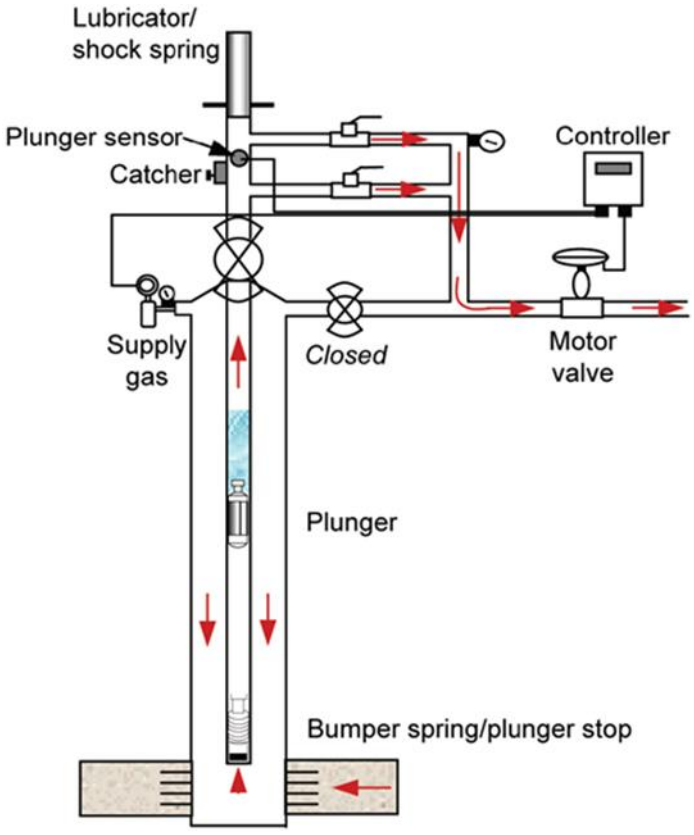

Figure 1.1: Schematic of a typical plunger lift installation (http://petrowiki.org/Plunger lift installation and maintenance)

Plunger lift has the characteristics of simple equipment, less investment, and low operating costs. It has become the first choice for oil wells with high gas-oil ratio and low energy production, and also the ideal alternative for continuous gas lift. At the same time, it is also very economical and reliable for drainage gas production of gas wells. The energy of the plunger pump system

comes from the natural buildup of pressure in the shut-in time and the gas velocity in the well. The plunger lift cycle starts from the plunger is released from the surface lubricator or released from the top of the bottom-hole bumper spring. After the surface valve is closed and the shut-in time begins, the plunger falls through the fluid to the bottom-hole bumper spring. When the valve opens, the plunger is launched from the bottom-hole bumper to the lubricator, bringing the gas and liquid to the surface. Plunger lift uses a free-piston that travels up and down the tubing string and acts as an interface between liquid and gas. Because the plunger provides a seal between the liquid and the gas, the well uses its energy to lift liquids out of the wellbore economically and efficiently. Plunger lift models can be broadly categorized into static and dynamic models.

1.1 Static Models

Static models use a semi-empirical correlation of the variables of interest for a particular part or stage of the process. Although the semi-empirical model is only an approximation, it can be used to estimate the conditions for opening or closing the production valve. Foss and Gaul developed a static model. The data of 100 wells in Ventura oilfield are used and there are three basic variations of plunger lift method in the wells to be analyzed (conventional plunger without packer, plunger-gas lift with packer and gas-lift valve, plunger lift with packer and standing valve, open mandrel on bottom). The sum of the forces acting on the plunger, and the minimum casing head pressure required to lift the plunger to the ground was obtained. The rising and falling velocities of the plunger were assumed constant. The weight of the gas column, plunger friction, and liquid drop were ignored. The minimum pressure required to maintain a liquid plug above the plunger was calculated. The assumption also included a 1000 ft/min rise velocity determined from field data and a 2000 ft/min fall velocity for the plunger through the gas. The plunger fall velocity

through the liquid was assumed to be 172 ft/min. These plunger velocities were used to determine plunger cycle time and the production of the well. Foss and Gaul showed that the cycle frequency depends on the productivity index (PI) of the well, available gas energy, tubing backpressure and plunger travel time. Attempts have been made to improve the Foss and Gaul model by changing values of liquid load, plunger average velocity, tubing pressure, and casing pressure, etc. Hacksma (1972) identified the optimal plunger cycle as the gas lifting the plunger and liquid slug to the surface as soon as the plunger falls back to the bottom-hole bumper. This work is still widely used in the design of plunger lifting.

1.2 Dynamic Models

The first dynamic model was developed by Lea (1982). Compared to static models, the dynamic model needs lower operating pressures and less gas than the static model. Lea analyzed plunger lift systems in oil wells with high gas-liquid ratio (GLR) or gas wells with limited liquid production. Gas and liquid frictions were considered in the plunger movement equations. However, it neglected gas leakage and liquid fallback from the plunger. Lea gave a simplified correlation for liquid loading as a function of time for a predominantly gas-flowing well. The plunger circulation of tight gas wells was simulated by a reservoir model. The results showed that the specified gas production times with plunger fixed on the surface have little effect on the average circulation production due to a certain balance effect. If the build-up period is longer than that required to lift the slugs, the production will be reduced. Compared with Foss and Gaul (1965) model, Lea model predicted 16% lower gas requirement with constant plunger rising and falling velocities to lift the plunger.

Marcano and Chacín (1994) proposed a comprehensive mechanistic (phenomenological) model of conventional plunger lift installations that contains all relevant stages of the production cycle (plunger rise, plunger fall, pressure buildup). The model includes the influence of the reservoir performance, overcoming the limitations of the static model. Marcano and Chacín model can predict the conventional plunger lift process by incorporating the liquid fallback during plunger rises as a linear function of average rising velocity. The field data used by Marcano and Chacín show that the model can reflect the production performance of the studied oil well, especially correctly reproduce the shape of the ratio of the fall-back to the driving pressure on the plunger. The difference between liquid/gas production and model prediction is between 15% and 20%. This result is encouraging because of the difficulties in obtaining accurate field measurements. Marcano and Chacín developed a computer program afterward, which can be used in the design and troubleshooting of a conventional plunger lifting. Results showed that under given conditions, where enough pressure is built up in the annulus for a complete plunger movement, the maximum production can be obtained. As long as the amount of gas from the reservoir is greater than the minimum requirement, the maximum production can be achieved regardless of the producing gas-liquid ratio. In other words, when enough gas and pressure is accumulated in the annulus, higher gas production rate can be obtained with a faster plunger cycle. The main difficulty of Marcano and Chacín's model in verifying and improving the production process is to obtain representative high-quality field data. Great efforts were made by Marcano and Chacín to acquire data for their study, but little was achieved. Only two producers with reasonably complete data sets were found.

Gasbarri and Wiggins (2001) developed a dynamic plunger lift model which incorporates reservoir performance correlations. They studied the effect of friction between the liquid slug and

tubing wall. The effect of the expanding gas above and below the plunger was also analyzed. In addition, the effect of separator and flow line was considered by including the transient behavior after liquid slug arrival to surface. The model contains four parts: upstroke, blowdown, buildup and reservoir components. In the upstroke component, the transient behavior of the gas at the top of the slug was included to simulate the behavior of the slug to the flow line when the tubing valve was opened. The model was tested by Gasbarri and Wiggins using the data from the example well of Lea (1982) and field case of Baruzzi (1995). The model prediction accurately matched the data from the example well of Lea and the field case well from Baruzzi. Compared with Lea's work, Gasbarri and Wiggins concluded that the transient behavior of gas expansion at the top of the slug has a substantial impact on the plunger velocity of the gas well when the tubing valve opens. Besides, the blowdown stage has a great influence on the results of upstroke velocity, slug size, and casing pressure. According to their study, the model can be used in the research of a plunger lift system, which provides a useful tool for system design and analysis.

Gupta et al. (2017) proposed a dynamic plunger lift model combining the fluid flow with the motion of the plunger. It considered the opening and closing of the surface valve and the plunger movement in the tubing string. Through a hybrid system model (HSM), the plunger lift system became a unified framework to efficiently discrete events and continuous dynamics. In the framework of HSM, the plunger lift process has been divided into six stages: plunger fall (gas), plunger fall (liquid), buildup, plunger rise, slug arrival, after-flow. The plunger moved through a 10000 feet tubing string, pushed by the pressure and flow below it. This model can run multiple cycles and evaluate the performance of the plunger. It quantitatively reproduces the typical observation characteristics of a plunger lift system, as well as captures the uncertainty of reservoir characteristics, wellbore, and production line through various model parameters and disturbances.

The model can be adjusted using standard surface measurements and reservoir performance parameters.

Although many plunger lifting models have been introduced in the literature, there is no universally validated model for the transient behavior of the gas, liquid, and plunger in the whole process of plunger lifting. Due to the oversimplification or incomprehensiveness of the assumption of plunger dynamics, the applicability of most existing models is questionable. This problem can be solved and the dynamic plunger lift model can be improved by introducing better closure relationships and making parametric studies to find the most suitable combination. The model developed in this study uses less assumptions. It combines reservoir performance by using Vogel's Inflow Performance Relationship (IPR) to obtain the flow of fluids from the reservoir to the well-bore. The present model also accounts for the modification of hydrocarbon mixture, which provides more accurate and reasonable predictions of tubing pressure and casing pressure.

CHAPTER 2

MODEL DEVELOPMENT

The plunger lift model proposed in this study comprises six different stages: plunger upstroke, gas blowout, plunger fall-down, pressure buildup, gas flows above and below plunger. The gas flow transient behavior in the tubing and reservoir performance is continuously modeled in a complete plunger lift cycle. In the stage of pressure buildup, reservoir performance makes contributions to restoring energy in the well bore. While in the plunger upstroke and fall-down stages, the gas flow behavior and its effect are calculated to obtain the plunger movement. The plunger lift simulation model is developed based on mass and momentum conservation equations of gas, liquid, and plunger. Based on Gasbarri and Wiggins's (2001) study, Zhu et al. (2017a, 2019f, and 2019j) applied several conservation momentum equations to the stages of plunger upstrokes and gas flow behavior. The proposed model is futher improved in this study.

2.1 Model Description and Assumptions

Based on Gupta et al. (2017) modeling framework of plunger lift, 9 variables can be used to describe the state of the plunger movement. Figure 2.1 (a) shows the schematic of the plunger lift variables. In this schematic, m_{g_a}, $m_{g_{tt}}$, m_{tb} denote gas mass in the annulus, above tubing, and below tubing, respectively. Similarly, m_{l_a}, $m_{l_{tt}}$, $m_{l_{tb}}$ represent liquid mass in the annulus, above tubing, and below tubing, respectively. X_p, V_p record plunger position and velocity in the tubing.

In Figure 2.1 (b) and (c), intermediate variables are used to describe plunger movement during the upstroke and blowout stages.

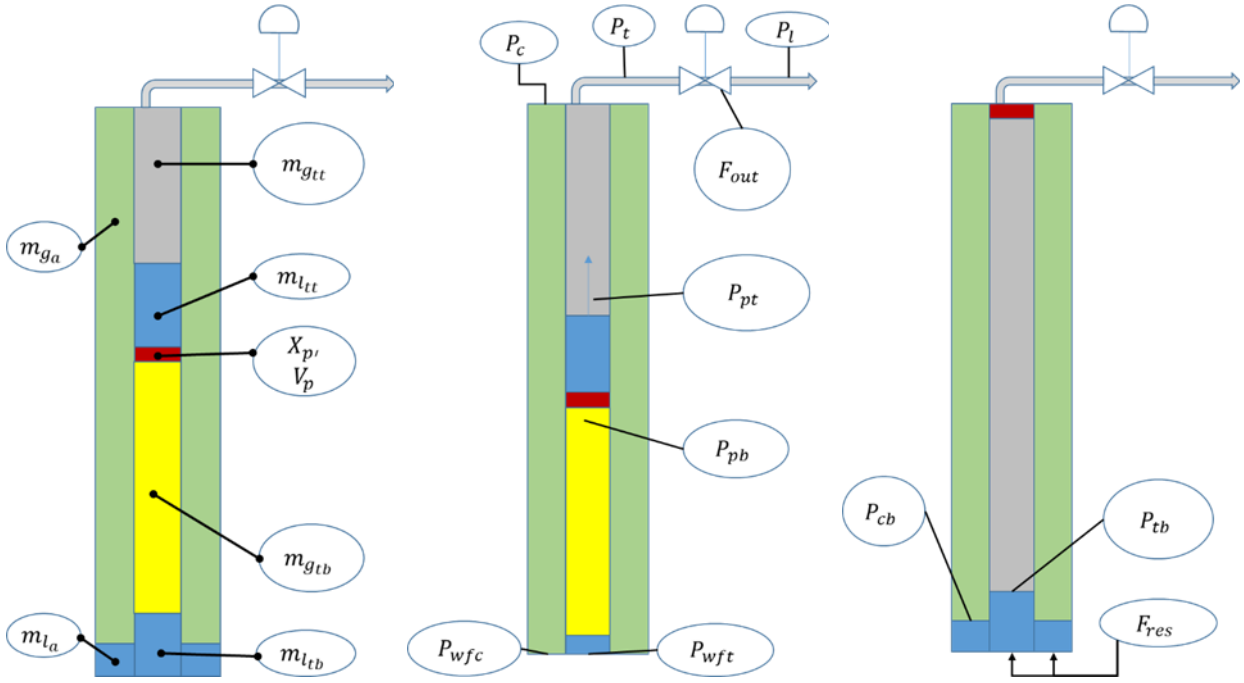

Figure 2.1: Schematic of plunger lift variables, (a) state variables, (b) intermediate variables in upstroke, (c) intermediate variables in blowout

Here, F_{out}, F_{res} are the gas mass flow rate at the surface and from the reservoir, respectively. P_C, P_t, P_l represent the casing pressure, tubing pressure, and surface line pressure. P_{wfc} and P_{wft} denote the bottom hole pressure in casing and tubing. P_{pt}, P_{pb} in Figure 2 (b) are the pressure above and below plunger, respectively. P_{cb} and P_{tb} are casing pressure and tubing pressure at the well bottom.

The reservoir performance, which is also known as inflow performance relationship, describes the relationship between the flow from the reservoir and the bottom hole pressure. Gas and liquid can flow into tubing and annulus through perforations between reservoir and bottom-hole. Because of the well completion, gas and liquid can flow only from annulus to tubing and cannot flow in the opposite direction. In this study, the transient inflow performance relationship

(IPR) of a gas reservoir is applied in the plunger lift model. The Rawlings and Schellhardt (1935) model is chosen to describe the IPR of a gas well:

$$Q_g = A - \frac{B}{C} \tag{1}$$

where

$$A = \frac{\frac{\mu Z}{\pi k h}\left(\frac{P_{SC}T}{T_{SC}Z_{SC}}\right) log\left(\frac{R_e}{R_w}\right)}{2\rho_{g,SC}\left(\frac{Z}{2\pi^2 h^2}\right)\left(\frac{P_{SC}T}{T_{SC}Z_{SC}}\right)\left(\frac{1}{R_w}-\frac{1}{R_e}\right)} \tag{2}$$

$$B = \sqrt{\frac{\frac{\mu Z}{\pi k h}\left(\frac{P_{SC}T}{T_{SC}Z_{SC}}\right) log\left(\frac{R_e}{R_w}\right)}{2\rho_{g,SC}\left(\frac{Z}{2\pi^2 h^2}\right)\left(\frac{P_{SC}T}{T_{SC}Z_{SC}}\right)\left(\frac{1}{R_w}-\frac{1}{R_e}\right)}} \tag{3}$$

$$C = 2\rho_{g,SC}\left(\frac{Z}{2\pi^2 h^2}\right)\left(\frac{P_{SC}T}{T_{SC}Z_{SC}}\right)\left(\frac{1}{R_w}-\frac{1}{R_e}\right) \tag{4}$$

where μ is gas viscosity in cp, Z is gas compressibility, k is gas permeability in md, h is the pay zone thickness in m, T is local temperature in K, R_e is the radius of drainage area in m, R_w is the radius of the wellbore in m, ρ is density in kg/m^3, subscript SC represents standard condition, and subscript g represents gas phase.

Specifically, if Eq. (2) is not a non-real number, Eq. (1) is reduced to

$$Q_g = \frac{(P_e^2 - P_w^2)}{\frac{\mu Z}{\pi k h}\left(\frac{P_{SC}T}{T_{SC}Z_{SC}}\right) log\left(\frac{R_e}{R_w}\right)} \tag{5}$$

where P_e is reservoir pressure in Pa, P_w is bottom pressure in Pa. For unsteady-state flow, gas mass production rate is a function of reservoir pressure, well pressure, well temperature, gas compressibility, reservoir permeability, pay zone thickness, well radius and oil viscosity. Thus,

$$Q_g = \frac{(P_R^2 - P_w^2)}{\left(\frac{\mu}{2\pi h k}\right)\left(\frac{PZT}{T_{sc}Z_{sc}}\right) log\left(\frac{2.25kt}{\mu C_t R_w^2}\right)} \tag{6}$$

where C_t is the total compressibility in psi^{-1}. Then, the inflow mass flow rates from the reservoir can be obtained by:

$$F_{g_{res}} = \rho_{g,SC} \cdot Q_g \tag{7}$$

$$F_{l_{res}} = \frac{F_{g_{res}}}{GLR} \tag{8}$$

where *GLR* is the gas-liquid ratio, kg/kg.

2.2 Geothermal and Pressure Gradient

In this study, a linear geothermal relationship is used to correlate temperature versus depth:

$$T_x = T_0 + \frac{\partial T}{\partial h} \Delta H \tag{9}$$

Typically, the temperature gradient for a formation is around 30 K per 1 km. Subscripts 0 corresponds to surface, and *x* is the target formation depth. The static gas column pressure depends on whether it is closed or not. For a specific gas column with a length L_g, the static pressure is calculated as:

$$P_{bottom} = P_{top} \cdot e^{\alpha L_a} \tag{10}$$

where α is in a function of the average compressibility (Z) and temperature (T) in each subsection of a well:

$$\alpha = \frac{M_g g}{ZRT} \tag{11}$$

In the gas flow out stage, the static pressure of the gas column needs to include the gas expansion effect. From previous studies (Maggard et al., 2000; Maggard, 2001):

$$P_{bottom}^2 = P_t^2 \cdot e^{2\cdot\alpha L_{tt}} + b^2 \cdot q_{g_{out}}^2 (e^{2\cdot\alpha L_{tt}} - 1) \tag{12}$$

where q_{gout} is the gas blowout flow rate at the surface in sm^3/s and b^2 can be expressed as:

$$b^2 = \frac{8g}{\pi^2 \alpha^2 d_t^5} f_g \tag{13}$$

where d_t is the tubing inner diameter in m and f_g is gas friction factor, which can be determined by Churchill (1977) equations as below:

$$A = \left[2.457\, ln\left(\frac{1}{\left((\frac{7}{Re})^{0.9} + 0.27\frac{\varepsilon}{D}\right)}\right)\right]^{16} \tag{14}$$

$$B = \left(\frac{37530}{Re}\right)^{16} \tag{15}$$

$$f = 2\left[\left((\frac{8}{Re})^{12} \frac{1}{(A+B)^{1.5}}\right)\right]^{1/12} \tag{16}$$

2.3 Fluid Properties

In order to calculate the integral of the pressure gradient, it is necessary to determine the velocity, density, and viscosity of each phase. In addition, it is necessary to determine the surface tension under different temperatures and pressures in some cases. When the fluid flows unsteadily in the tubing and annulus, the temperature and pressure of the fluid also change continuously (Zhu 2019). Therefore, extremely active mass transfer occurs between the liquid and gas phases. When the pressure is lower than the bubble point pressure, the gas escapes from the oil as the bottom hole pressure decreases, thus increases the gas velocity, oil density, and viscosity. Compositional model and black-oil model can be used to predict the changes of the flow rate and fluid properties

to calculate the integral of the pressure gradient equation (Zhu et al. 2018d and 2018e). The black-oil model assumes that the API gravity of the liquid phase, gas specific gravity, gas solubility, and formation volume factor are fixed at certain temperature and pressure. Under this assumption, the composition of oil and gas will not change with temperature and pressure. Assuming that the composition is constant the model can be effective and accurate to predict the physical properties of the liquid phase. However, there are errors and deviations in the gas phase properties prediction. The obvious limitation of the black-oil model is the inability to predict retrograde condensation phenomena. The black-oil model should be avoided for very volatile or light crude oil and gas condensates. As a result, compositional models are recommended for these cases.

2.3.1 Flash Calculations

The equilibrium constant for component *i*:

$$K_i = \frac{y_i}{x_i} \tag{17}$$

The overall material balance is:

$$F = L + V \tag{18}$$

where F is the number of moles of feed or mixture, L is the number of moles of liquid, V is the number of moles of vapor.

Individual component balances are:

$$z_i = x_i L + y_i V \tag{19}$$

where z_i is the mole fraction of component i in feed, x_i is the mole fraction of component i in liquid, y_i is mole fraction of component i in vapor.

When Eq. (17) is divided by *F*, it can be written as:

$$\frac{L}{F} = 1 - \frac{V}{F} \tag{20}$$

In order to solve the mole fraction of liquid component *i*, Eq. (18) is solved for x_i, and y_i and $\frac{L}{F}$ are replaced by Eq. (17) and Eq. (20). As a result, Eq. (21) is given as:

$$x_i = \frac{z_i F - y_i V}{L} = \frac{z_i - y_i \frac{V}{F}}{\frac{L}{F}} = \frac{z_i - x_i K_i \frac{V}{F}}{1 - \frac{V}{F}} \tag{21}$$

Equation (21) can be re-written as:

$$x_i = \frac{z_i}{1 + \frac{V}{F}(K_i - 1)} \tag{22}$$

Similarly, vapor mole fraction can be solved by using equilibrium definition as:

$$y_i = x_i K_i = \frac{z_i K_i}{1 + \frac{V}{F}(K_i - 1)} \tag{23}$$

The sum of mole fractions is:

$$\sum_{i=1}^{n} x_i = \sum_{i=1}^{n} y_i = 1.0 \tag{24}$$

Therefore,

$$\sum_{i=1}^{n}(y_i - x_i) = \sum_{i=1}^{n} \frac{z_i(K_i - 1)}{(K_i - 1)\frac{V}{F} + 1} = f\left(\frac{V}{F}\right) = 0 \tag{25}$$

Equation (25) can be solved by the Second-order Newton convergence scheme. The following parameters are required:

- Number of components, *n*
- Mole fraction of each component in the mixture, z_i
- The equilibrium constant for each component, K_i
- First guess for the mole ratio, $\left(\frac{v}{F}\right)_j = 0.5$

The ratio *V/F* can be improved by using Newton-Raphson method as:

$$\left(\frac{V}{F}\right)_{j+1} = \left(\frac{V}{F}\right)_j - \frac{f(V,F)_j}{\left(\frac{df}{d(V/F)}\right)_j} \tag{26}$$

where the derivative, $\left(\frac{df}{d(V/F)}\right)_j$ can be obtained by differentiating Eq. (25) with respect to *V/F*:

$$\left(\frac{df}{d(V/F)}\right)_j = -\sum_{i=1}^{n} \frac{z_i(K_i - 1)^2}{[(K_i - 1)\left(\frac{V}{F}\right)_j + 1]^2} \tag{27}$$

Convergence is achieved when:

$$\left|\left(\frac{v}{F}\right)_{j+1} - \left(\frac{v}{F}\right)_j\right| < 1.0 \times 10^{-6} \tag{28}$$

When *V/F* is converged, the composition of each phase can be determined by Eq. (22) and Eq. (23). The procedure requires the value for K_i at the pressure and temperature of interest. *K* values can be determined from the equation of states (EOS)

2.3.2 Equilibrium Constant

For the ideal gases, the total system pressure in a confined system is equal to the summation of the partial pressures (the pressure when the individual component exists alone in the system) of each component (Dalton's Law). Then, the total pressure in the system and the liquid component are:

$$p = \sum_{i=1}^{n} p_i \tag{29}$$

$$y_i = \frac{p_i}{p} \tag{30}$$

The partial pressure of the i^{th} component in the vapor phase in the ideal solution is equal to the product of mole fraction of the i^{th} component in the liquid phase and the vapor pressure of the pure i^{th} component (Raults' Law). Therefore, the partial pressure of the component can be written as:

$$p_i = x_i p_{vi} \tag{31}$$

where *p* is total system pressure, p_{vi} is the vapor pressure of component *i*, p_i is the partial pressure of component *i*.

Combining Eq. (29) to (31), the equilibrium constant can be written as:

$$K_i = \frac{p_{vi}}{p} = \frac{y_i}{x_i} \tag{32}$$

However, *K* is a function of not only the pressure and temperature but also the composition of the hydrocarbon phases for real gases. *K* values can be obtained using the equation of state (EOS). The *K* values is estimated by Wilson's correlation as:

$$K_i = \frac{p_{ci}}{p} \exp\{5.37(1 + w_i)\left[1 - \frac{T_{ci}}{T}\right]\} \tag{33}$$

where *w* is the acentric factor. For pure components, *w* can be calculated as:

$$w = -log p_{v,p_r}(at\ T_r = 0.7) - 1.0 \tag{34}$$

2.3.3 Fugacity

In the plunger lift model calculation, it is unrealistic to use the ideal gas model. At local pressure and temperature, the liquid mixture in the tubing and casing is in equilibrium with the vapor mixture. The key parameters to determine the phase behavior are pressure, temperature, and the components of the liquid phase and vapor phase. An important objective for flash calculation is to determine the individual phase compositions, pressure and temperature at the computation node, and the overall mixture composition. The equilibrium constants depend on all these parameters, i.e., *K*=f (p, T, z_i).

The equilibrium constant can be calculated by the thermodynamics of vapor-liquid equilibrium. This equilibrium is related to the fugacity of each component. The mass transfer of these components in each phase is zero when the fugacity of each component is equal. Thus the thermodynamic equilibrium is achieved. According to thermodynamic vapor-liquid equilibrium, the fugacities of every component *i* in each phase should be identified as:

$$f_i^V = f_i^L \tag{35}$$

where *f* is fugacity, superscript *V* and *L* are for vapor phase and liquid phase, respectively.

The fugacity of pure components can be calculated as:

$$f = pexp[\int_0^p (\frac{Z-1}{p})dp] \tag{36}$$

The ratio of the fugacity to the system pressure is called the fugacity coefficient ϕ. At equilibrium, the fugacity coefficient of component *i* in each phase is a function of the system pressure, temperature, and phase composition. In mixtures, ϕ of any component is defined as:

$$\phi_i^L = \frac{f_i^L}{(x_i p)} \tag{37}$$

$$\phi_i^v = \frac{f_i^V}{(y_i p)} \tag{38}$$

where ϕ_i^v is the fugacity coefficient of component *i* in the vapor phase and ϕ_i^L is the fugacity coefficient of component *i* in the liquid phase. Therefore, the equilibrium constant *K* can be found by:

$$K_i = \frac{y_i}{x_i} = \frac{\phi_i^L}{\phi_i^v} \tag{39}$$

2.3.4 Equation of State (EOS)

The fugacity coefficient of each component in each phase is defined by using equation of state. EOS is an analytical expression of pressure, temperature and molar volume of fluids. A generalized form for a cubic EOS is:

$$p = \frac{RT}{V - b} = \frac{a}{V^2 + ubV + wb^2} \tag{40}$$

Equation (40) can also be written as:

$$Z^3 - (1 + B - uB)Z^2 + (A + wB^2 - uB - uB^2)Z - AB - wB^2 - wB^3 = 0 \tag{41}$$

where

$$A = \frac{ap}{R^2T^2} \tag{42}$$

$$B = \frac{bp}{RT} \tag{43}$$

where *p* is the system pressure, Pa; *T* is system temperature, K; *R* is gas constant that is 2.49 MPa-dm^3/kg-mole, *V* is molar volume in dm^3/mole, *a* is a measure of the intermolecular attractive forces between the molecules, *b* is known as co-volume that represents the volume of molecules. There are four well-known cubic EOS: van der Waals, Redlich-Kwong (RK), Soave-Redlich-Kwong (SRK), and Peng-Robinson (PR). In the proposed plunger model, Peng-Robinson (PR) EOS is selected. In Peng-Robinson EOS, *u* equals to 2 and *w* equals to -1. *a* and *b* are calculated based on van der Waals' observation, where the critical isotherm has a zero slope and an inflection point at the critical point:

$$\left(\frac{dp}{dV}\right)_{T_c} = 0 \tag{44}$$

$$\left(\frac{d^2p}{dV^2}\right)_{T_c} = 0 \tag{45}$$

The Peng-Robinson (PR) Equation of State cubic equations are:

$$Z_L^3 - (1 - B_L)Z_L^2 + Z_L(A_L - 2B_L - 3B_L^2) - (A_L B_L - B_L^2 - B_L^3) = 0 \quad (46)$$

$$Z_V^3 - (1 - B_V)Z_V^2 + Z_V(A_V - 2B_V - 3B_V^2) - (A_V B_V - B_V^2 - B_V^3) = 0 \quad (47)$$

where Z_L represents the liquid-phase compressibility factor and Z_V represents the vapor-phase compressibility factor.

The fugacity coefficients for Peng-Robinson (PR) Equation of State are:

$$ln\phi_i^L = \left(\frac{b_i}{b}\right)_L (Z_L - 1) - \ln(Z_L - B_L) - \frac{A_L}{B_L}[2\left(\frac{a_i}{a}\right)_L^2 - \left(\frac{b_i}{b}\right)_L]\ln(1 + \frac{B_L}{Z_L}) \quad (48)$$

$$ln\phi_i^V = \left(\frac{b_i}{b}\right)_V (Z_V - 1) - \ln(Z_V - B_V) - \frac{A_V}{B_V}[2\left(\frac{a_i}{a}\right)_V^2 - \left(\frac{b_i}{b}\right)_V]\ln(1 + \frac{B_V}{Z_V}) \quad (49)$$

where

$$\left(\frac{a_i}{a}\right)_L^{0.5} = \frac{a_i^{0.5} T_{ci}/p_{ci}^{0.5}}{\sum_{i=1}^n x_i\, \alpha_i^{0.5} T_{ci}/p_{ci}^{0.5}} \quad (50)$$

$$\left(\frac{a_i}{a}\right)_V^{0.5} = \frac{a_i^{0.5} T_{ci}/p_{ci}^{0.5}}{\sum_{i=1}^n y_i\, \alpha_i^{0.5} T_{ci}/p_{ci}^{0.5}} \quad (51)$$

$$(\frac{b_i}{b})_L = \frac{T_{ci}/p_{ci}}{\sum_{i=1}^n x_i\, T_{ci}/p_{ci}} \quad (52)$$

$$(\frac{b_i}{b})_V = \frac{T_{ci}/p_{ci}}{\sum_{i=1}^n y_i\, T_{ci}/p_{ci}} \quad (53)$$

$$A_L = C_a \frac{p}{T^2}[\sum_{i=1}^n x_i\, T_{ci}\left(\frac{\alpha_i}{p_{ci}}\right)^{0.5}]^2 \quad (54)$$

$$A_V = C_a \frac{p}{T^2}[\sum_{i=1}^n y_i\, T_{ci}\left(\frac{\alpha_i}{p_{ci}}\right)^{0.5}]^2 \quad (55)$$

$$B_L = C_b \frac{p}{T} \sum_{i=1}^{n} x_i \, T_{ci}/p_{ci} \tag{56}$$

$$B_V = C_b \frac{p}{T} \sum_{i=1}^{n} y_i \, T_{ci}/p_{ci} \tag{57}$$

$$a_i = [1 + S_i\left(1 - T_{Ri}^{0.5}\right)]^2 \tag{58}$$

where C_a is equal to 0.45724, C_b is equal to 0.07780 and:

$$S_i = 0.37464 + 1.5422w_i - 0.26992w_i^2 \tag{59}$$

The equilibrium constant (*K*) can be calculated by Eq. (39)

2.3.5 Solution Procedure

Z factor equations are third-degree polynomial equations. The compressibility factor *Z* yields a single real root for the single-phase region. In the two-phase region, *Z* yields the largest root corresponds to the vapor phase z_v and the smallest root corresponds to the liquid phase z_L. *Z* factors used in the fugacity coefficient for each phase are composition dependent, which makes the equilibrium constants also composition dependent. The following is the solution procedure to calculate equilibrium constants.

1. Inputs include: *p*, *T* and the overall composition z_i for each component.
2. Estimate $K_{i,E}$ values for each component using Wilson's equation.
3. Based on $K_{i,E}$ and the known z_i values, perform flash calculations.
4. Determine the fugacity coefficients of each component in each phase using appropriate EOS.
5. Calculate $K_{i,C}$ values for each component using fugacity coefficient ratios (Eq. (39)).

6. Compare equilibrium constants in Step 2 with the calculated values in Step 5 using the following convergence criteria:

$$\sum_{i=1}^{n}[\frac{K_{i,C}}{K_{i,E}} - 1]^2 \leq \varepsilon \tag{60}$$

where ε is the pre-assigned convergence tolerance ($\leq 10^{-4}$) and n is the number of components in the system.

7. If the criterion in Step 6 is not satisfied, the calculated values are used as the new guesses and Steps 3-6 are repeated until convergence.

Based on the Peng-Robinson (PR) flash model, the calculation flow chart for equilibrium constants *Z* factor calculation is shown in Figure 2.2.

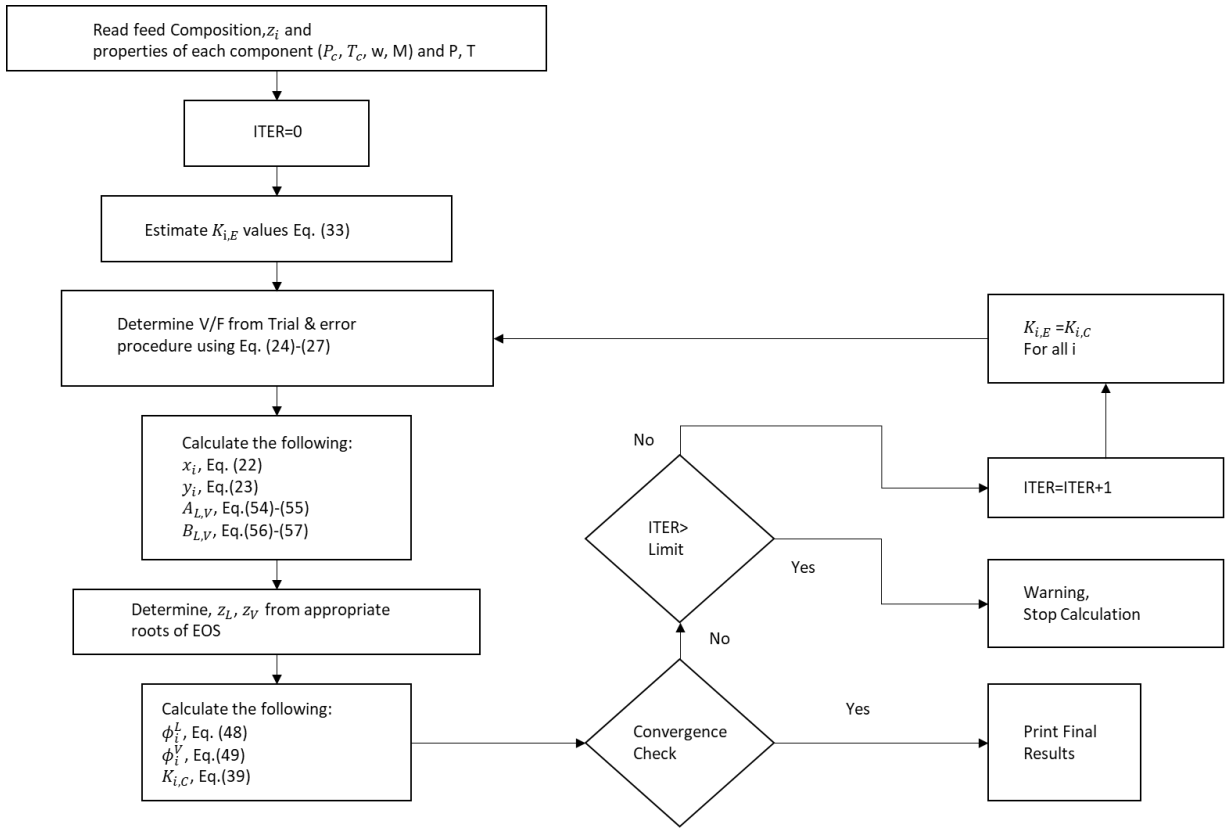

Figure 2.2: Flow chart to calculate equilibrium constants Z factor

2.3.6 Fluid Properties Correlations

The vapor phase and liquid densities can be calculated by:

$$\rho_V = \frac{p\sum_{i=1}^{n} y_i M_i}{Z_v RT} \tag{61}$$

$$\rho_L = \frac{p\sum_{i=1}^{n} x_i M_i}{Z_L RT} \tag{62}$$

where M_i is the molecular weight of the i^{th} component. At the bubble point curve, $z_i \approx x_i$. Then the liquid phase component mole fraction can be calculated as:

$$y_i = \mathrm{z_i K_i} \tag{63}$$

$$\sum_{i=1}^{n} y_i = \sum_{i=1}^{n} z_i K_i = 1 \tag{64}$$

The procedure to calculate the bubble point is:

1. Guess a bubble point pressure using:

$$1 = \sum_{i=1}^{n} z_i \frac{p_{ci}}{p_b} \exp\{5.37(1+w_i)\left[1-\frac{T_{ci}}{T}\right]\} \tag{65}$$

$$p_b = \sum_{i=1}^{n} z_i p_{ci} \exp\{5.37(1+w_i)\left[1-\frac{T_{ci}}{T}\right]\} \tag{66}$$

2. Determine *K* values by EOS
3. Check the above criterion
4. Continue the iteration until the convergence:

If Eq. (67) is satisfied, the assumed bubble pressure is high and the next guess must be a lower pressure.

$$\sum_{i=1}^{n} z_i K_i < 1 \tag{67}$$

On the contrary, if Eq. (68) is satisfied, the assumed bubble pressure is low and the next guess must be a higher pressure.

$$\sum_{i=1}^{n} z_i K_i > 1 \tag{68}$$

At the Dew point, where L=0 and V=F, and $z_i = y_i$. Equation (23) reduces to:

$$x_i = \frac{z_i}{K_i} \tag{69}$$

$$\sum_{i=1}^{n} x_i = \sum_{i=1}^{n} \frac{z_i}{K_i} = 1 \tag{70}$$

The procedure to calculate the dew point is:

1. Guess a dew point pressure using

$$p_d = \frac{1}{\sum_{i=1}^{n} \frac{z}{p_{ci} \exp\{5.37(1+w_i)\left[1-\frac{T_{ci}}{T}\right]\}}} \tag{71}$$

2. Determine K values using an EOS
3. Check the above criterion
4. Continue the iteration until the convergence. If Eq. (72) is satisfied,

$$\sum_{i=1}^{n} \frac{z_i}{K_i} > 1 \tag{72}$$

the assumed dew pressure is higher andthe next guess must be a lower pressure. If the following equation satisfied,

$$\sum_{i=1}^{n} \frac{z_i}{K_i} < 1 \tag{73}$$

the assumed bubble pressure is lower and the next guess must be a higher pressure.

The additional calculations can then be made for liquid density ρ_L, liquid viscosity μ_L, gas viscosity μ_g and liquid surface tension σ_L. Hankinson and Thomson (1979) correlation is used for liquid density ρ_L. The Bray and Clark (1964) correlation is used to compute liquid viscosity μ_L. Lee et al. (1975) correlation is used to calculate gas viscosity. Finally, the liquid surface tension can be calculated by Weinaugz and Katz (1943) correlation.

2.4 Load Factor

Before the surface valve opens, it is extremely important to check whether the casing pressure is high enough and other well conditions such as liquid loading in order to optimize the production. First, the well needs to be clean. If there is too much liquid at the bottom, the well needs to be shut-in for a few days to allow building enough pressure, which can help push the liquid to the surface.

The Load Factor can be used to check whether the well is ready to be opened. The surface valve can be opened and the plunger will be shot from the tubing shoe only after the Load Factor condition is satisfied. This procedure can be operated automatically or manually. The definition of the Load Factor is:

$$Load\ Factor = 100 \times \frac{Shut\text{-}in\ Casing\ Pressure - Shut\text{-}in\ Tubing\ Pressure}{Shut - in\ Casing\ Pressure - Line\ Pressure} \tag{73}$$

If Load Factor is less than 50%, the surface valve will be opened and the plunger can be shot from the bottom of the tubing.

It is necessary to wait until the well pressure meets the initial Load Factor requirements. If the valve opens too early, the well can not have sufficient energy to unload the accumulated liquid in the wellbore. Therefore, it is important for the well to buildup enough pressure before the production. If time permits, the shut-in should be allowed to proceed until the pressure is enough to ensure the first plunger lift cycle to be accomplished.

A common mistake is to open the valve longer than the requirement. When the casing pressure drops too low, the valve needs to be closed and the well should be shut-in to build up pressure. Whether the plunger can be lifted to the surface and unload the liquid effectively is an important criterion to determine if the well has accumulated enough energy.

In the shut-in stage of a plunger lift cycle, it is desirable to vent the gas above the liquid in the tubing to obtain a lower pressure to create higher differential pressure between plunger and slug, which helps remove the liquid and push the plunger to the surface. At the same time, shut-in should be maintained until enough pressure is built up. If the shut-in time is too short, the well can be killed by the liquid loading. The aim of using the Load Factor is to ensure that the well will not be killed by less enough shut-in time.

2.5 Upstroke

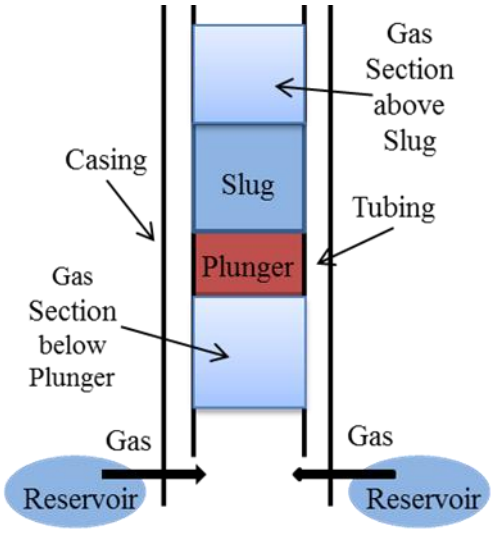

Figure 2.3: Plunger, liquid slug, and gas sections below and above plunger

The flow from tubing to the annulus and from the wellbore to the reservoir is assumed to be zero at the well bottom. Thus:

$$F_{g_{ann}} = F_{g_{res}} - F_{g_{tub}} \tag{74}$$

$$F_{l_{ann}} = F_{l_{res}} - F_{l_{tub}} \tag{75}$$

where subscripts *ann*, *res*, *tub* correspond to the annulus, reservoir, and tubing. The flow rate is positive if the fluid flows into that section.

When the surface control valve opens, the gas section above the slug has an outflow rate q_{gout}, which can be determined by the standard valve equation as:

$$q_{g_{out}} = \begin{cases} C_v \cdot P_t & P_t \geq 2P_l \\ 2C_v\sqrt{(P_t - P_l)P_l} & P_l < P_t < 2P_l \end{cases} \tag{76}$$

where P_l is the surface production line pressure (Pa), and C_v is the valve coefficient. According to Eq. (12), the static pressure in the gas column above the plunger can be obtained through:

$$P_t = m_{g_{tt}} \frac{Z_t RT}{A_t(H - X_p - L_{tt})M_g} \tag{77}$$

$$P_{pt}^2 = P_t^2 \cdot e^{2\cdot\alpha(H-X_p-L_{tt})} + b^2 \cdot q_{g_{out}}^2 (e^{2\cdot\alpha(H-X_p-L_{tt})} - 1) \tag{78}$$

where L_{tt} is the liquid slug length above the plunger.

In the plunger upstroke stage, constant density is used in the momentum equations that are applied to single-phase liquid based on Lea (1982) model. The control volume in the moving system is assumed constant when the plunger and slug travel in the tubing. The acceleration of the slug can be obtained from the momentum equations. Figure 2.4 shows the forces acting on the slug and plunger in the tubing.

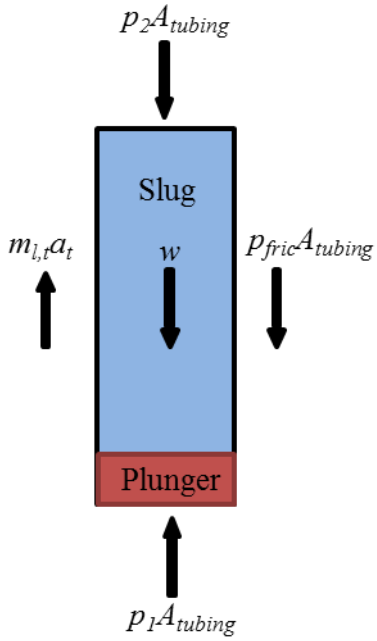

Figure 2.4: Force balance of plunger upstroke (plunger and slug in tubing)

Gasbarri and Wiggins (2001) developed an upstroke model for plunger lift, which has been applied in this study to describe plunger upward movement and gas behavior. When the plunger moves upward and the slug is far from the wellhead, the slug acceleration can be solved by the momentum equation in the vertical direction based on the force balance on the control volume as:

$$\frac{\partial V_p}{\partial t} = \frac{(P_{pb} - P_{pt} - P_{fric})A_t}{m_p + m_{l_{tt}}} - g \tag{79}$$

where V_p is the plunger velocity, m_p is the plunger mass, P_{fric} is the fiction pressure added to the liquid slug, which can be obtained by:

$$P_{fric} = \frac{1}{2}\rho_l V_p^2 f(\frac{L_s}{d_t}) \tag{80}$$

where f is the friction factor and can be calculated through Churchill correlation in Eq. (14).

Below the plunger, the reservoir fluid flows into tubing and annulus according to Eqs. (17) and (18). The bottom-hole pressure in both tubing (P_{wft}) and annulus (P_{wfa}) should be equal. P_{wft} in the tubing is calculated by the following equations:

$$p_{pb} = m_{g_{tb}} \frac{Z_t RT}{A_t(X_p - L_{tb})M_g} \tag{81}$$

$$p_{tb} = p_{pb} \cdot e^{\alpha(X_p - L_{tb})} \tag{82}$$

$$P_{wft} = p_{tb} + L_{tb}\rho_L g \tag{83}$$

Similarly, P_{wfa} in the annulus is calculated as:

$$P_c = m_{g_a} \frac{Z_c RT}{A_a(H - L_a)M_g} \tag{84}$$

$$P_{cb} = P_c \cdot e^{\alpha(H - L_a)} \tag{85}$$

$$P_{wfa} = P_{cb} + L_a\rho_L g \tag{86}$$

Since P_{wft} equals to P_{wfa}, the liquid flow rate from the reservoir to annulus F_{lann} can be solved.

No gas is above the plunger when the slug arrives at the surface. Therefore:

$$\frac{d}{dt}m_{gtt} = 0 \tag{87}$$

At the same time, the liquid slug starts to produce liquid at the flow rate F_{lout}:

$$F_{l_{out}} = V_p A_t \rho_l \tag{88}$$

Thus, the mass change of liquid slug above the plunger with time due to flow out of tubing can be calculated as:

$$\frac{d}{dt}m_{ltt} = -F_{l_{out}} \tag{89}$$

2.6 Gas Blowout

The gas blowout stage represents gas production when the wellhead valve is opened for a certain time after the plunger arrives to surface. In this stage, fluid is produced from the reservoir and liquid loads up at the well bottom. When the gas production is less than the required rate due to the loaded liquid, the valve needs to be closed and the blowout stage is completed. In this study, only single-phase gas flow is considered to simplify the calculation. Thus, the gas/liquid mass in the tubing changes due to the bottom inflow and surface outflow as:

$$\frac{d}{dt}m_{g_{tb}} = F_{g_{tub}} - F_{g_{out}} \tag{90}$$

$$\frac{d}{dt}m_{l_{tb}} = F_{l_{tub}} \tag{91}$$

The hydrostatic pressure of the gas column in the tubing is calculated by:

$$P_t = m_{g_{tb}} \frac{Z_t RT}{A_t (H - L_{tb}) M_g} \tag{92}$$

$$P_{tb}^2 = P_t^2 \cdot e^{2 \cdot \alpha (H - L_{tb})} + b^2 \cdot q_{g_{out}}^2 (e^{2 \cdot \alpha (H - L_{tb})} - 1) \tag{94}$$

2.7 Plunger Down-Stroke

In the plunger downstroke stage, the plunger moves downward from wellhead to the bottom after the gas blowout stage. The plunger falls once the gas blowout is finished. Due to the liquid accumulation at the bottom of the well, the plunger downstroke movement can be divided into two parts: travels in the gas phase and liquid phase. Therefore, the plunger accelerations in these two fluids must be formulated separately.

Generally, constant plunger falling velocities were used in previous plunger lift models. Gasbarri and Wiggins's (2001) model assumed the plunger falling velocity to be 1000 ft/min in the gas phase and 175 ft/min in the liquid phase. Nadkrynechny et al. (2013) proposed a detailed orifice-flow-based model, which indicates that the plunger reaches the terminal velocity quickly and falls at constant velocity thereafter until arriving at the bottom of the well. As can be seen in Figure 2.5, it shows the schematic of the plunger downstroke movement. The forces (gravity force and drag force) acting on the plunger are used to obtain plunger falling acceleration. Thus, if the plunger falls at a constant velocity, the gravity equals to drag force. Then, the plunger falling velocity is given by:

$$V_p = \frac{C_d}{\sqrt{\rho_q}} \cdot \frac{A_p}{A_t} \sqrt{\frac{2 M_p \cdot g}{A_t}} \tag{95}$$

where q is g or l for plunger falling in gas or liquid column. C_d is the drag coefficient.

Figure 2.5: Force balance for plunger downstroke

As pointed out by Nadkrynechny et al. (2013), the plunger falling process is less important than plunger upstroke, since the flow of fluids into the wellbore are not affected by plunger fall dynamics. Thus, the static pressure in tubing and annulus can be obtained by:

$$P_{tb} = (m_{g_{tb}} + m_{gtt}) \cdot \frac{Z_t RT}{A_t(H - L_{tb})M_g} \cdot e^{\alpha(H - L_{tb})} \tag{96}$$

$$P_{cb} = m_{g_a} \frac{Z_c RT}{A_a(H - L_a)M_g} \cdot e^{\alpha(H - L_a)} \tag{97}$$

Substituting Eqs. (38) and (39) into Eqs. (26) and (29), respectively, and recalling $P_{wft} = P_{wfa}$, the liquid that flows into tubing and annulus can be calculated. Especially, when the plunger falls into the tubing liquid column, the gas mass (m_{gtb}) below plunger is zero. Thus, the liquid mass change above and below plunger can be obtained by:

$$\dot{m}_{l_{tb}} = F_{l_{tub}} - V_p \rho_l A_t \tag{98}$$

$$\dot{m}_{l_{tt}} = V_p \rho_l A_t \tag{99}$$

2.8 Buildup

The energy buildup stage and reservoir performance are combined in the model. A seat at the bottom of the well is used to host the plunger. The energy buildup stage describes the accumulation of reservoir energy under the plunger seat at well bottom when the plunger is locked on it. When the reservoir energy (pressure) reaches a certain level, the seat locker will open and the plunger will start to travel upward again. In this stage, the plunger sits still, and the system has no moving part. The reservoir fluid enters both annulus and tubing. The static pressure can be calculated from the aforementioned equations.

CHAPTER 3

OLGA SIMULATION

The commercial software OLGA is widely used in literatures to validate the proposed model (Zhu et al., 2017b, 2018a, 2018b, 2019i, and 2019j). In this section, the plunger lift system is numerically studied using a commercial dynamic multiphase flow simulator (OLGA).

3.1 Well Trajectory and Geometries

Figure 3.1 shows the well trajectory corresponding with the well details, including the inner and outer diameters of the tubing and casing, reservoir position, etc. The well is a vertical well and its depth is around 3000 m (10000 ft). The parameters of the wellbore geometry are shown in Table 3.1. It should be noticed that a standing valve is positioned at the end of the vertical section of the tubing to prohibit the plunger from falling back into the wellbore or annulus. In reality, the plunger sits on top of the bumper spring after it falls back from the wellhead. The plunger parameters are shown in

Table 3.2.

Table 3.1: Wellbore geometrical parameters

Parameter	**Value**	**Unit**
Well depth	3000	m
Tubing ID	5.067	cm
Tubing OD	6.668	cm

Casing ID	12.319	cm
Absolute roughness	6.35E-04	cm

Table 3.2: Plunger geometrical parameters

Parameter	Value	Unit
Plunger mass	5	kg
Plunger length	0.4	m
Plunger diameter	4.826	cm
Plunger drag coefficient	0.457	-

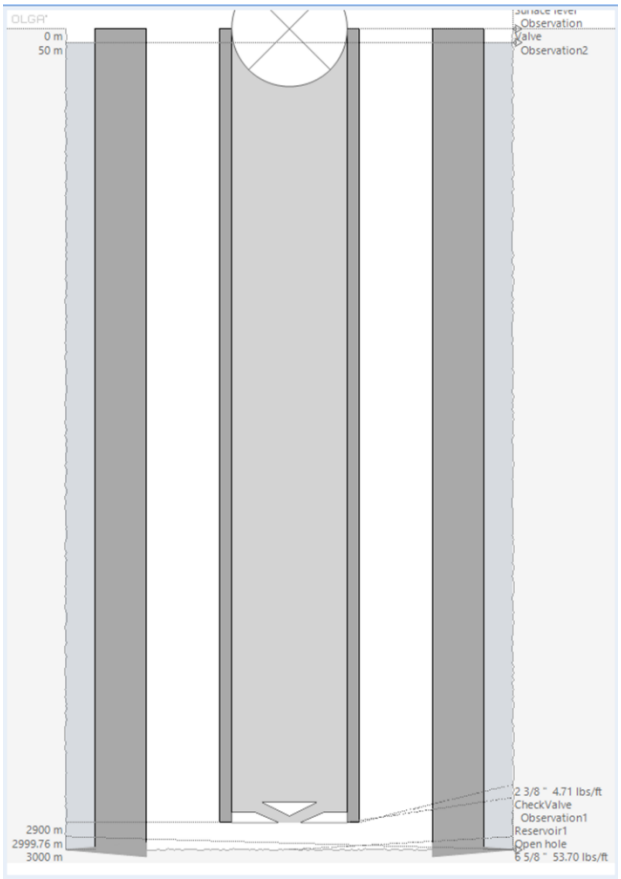

Figure 3.1: Well geometries

3.2 OLGA Simulation Inputs

The reservoir studied in OLGA simulation is the same as the one used in the proposed model. The backpressure method is incorporated to describe reservoir flow rates. The following IPR equation is used in gas wells:

$$q = C(p_R^2 - p_{wf}^2)^n \tag{100}$$

where *C* is defined by:

$$C = \frac{(0.703kh)^n}{(T\mu_g Z)^n D^{1-n}[\ln\left(\frac{r_e}{r_w}\right) - 0.75 + s]^{2n-1}} \tag{100}$$

Table 3.3 shows the input parameters for the reservoir model.

Table 3.3: Reservoir properties

P_R (Pa)	**T_R (C)**	**C ((scf/d)/psi)**	**n**	**CGR (Sm3/Sm3)**	**WGR (Sm3/Sm3)**
6000000	100	0.95	1	Table	0

The fluid was generated by the PVTsim Nova 4. In order to compare different gas properties, two different gas mixtures were generated using PVTsim Nova 4. One is light gas with 93% of methane, the other is relatively heavy gas containing only 61% methane and more heavier components (6.85% Heptane+).

Table *3.4* and Table 3.5 show the two types of fluids.

Table 3.4: Composition of light gas for OLGA

Component	Mol %	Molecular Weight	Critical Temperature (C)	Critical Pressure (MPa)	Normal Tb (C)
N2	0.130	28.014	-146.950	33.94	-195.750
CO2	0.180	44.010	31.050	73.76	-78.500
C1	93.000	16.043	-82.550	46.00	-161.550
C2	6.690	30.070	32.250	48.84	-88.550

Table 3.5: Composition of heavy gas for OLGA

Component	Mol %	Mol Wt
CO2	0.18	44.010
C1	61.920	16.043
C2	14.080	30.070
C3	8.350	44.097
iC4	0.970	58.124
nC4	3.410	58.124
iC5	0.840	72.151
nC5	1.480	72.151
C6	1.790	86.178
C7+	6.850	143.000

The phase envelop generated by PVTsim is shown in Figure 3.2 and Figure 3.3. Compared to the heavy gas, the phase envelope of the light gas shifts to the left-hand-side, which indicates that limited gas condensation is formed during the plunger cycles. On the other hand, the phase envelope of the heavy gas is shifted to the right, which proves the existence of liquid and gas condensation.

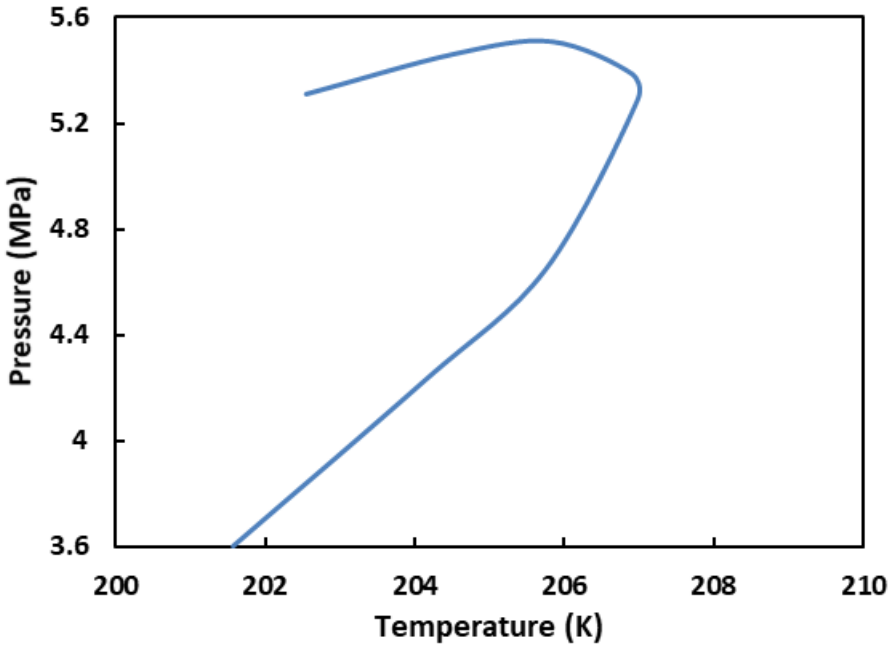

Figure 3.2: Phase envelop of the light gas

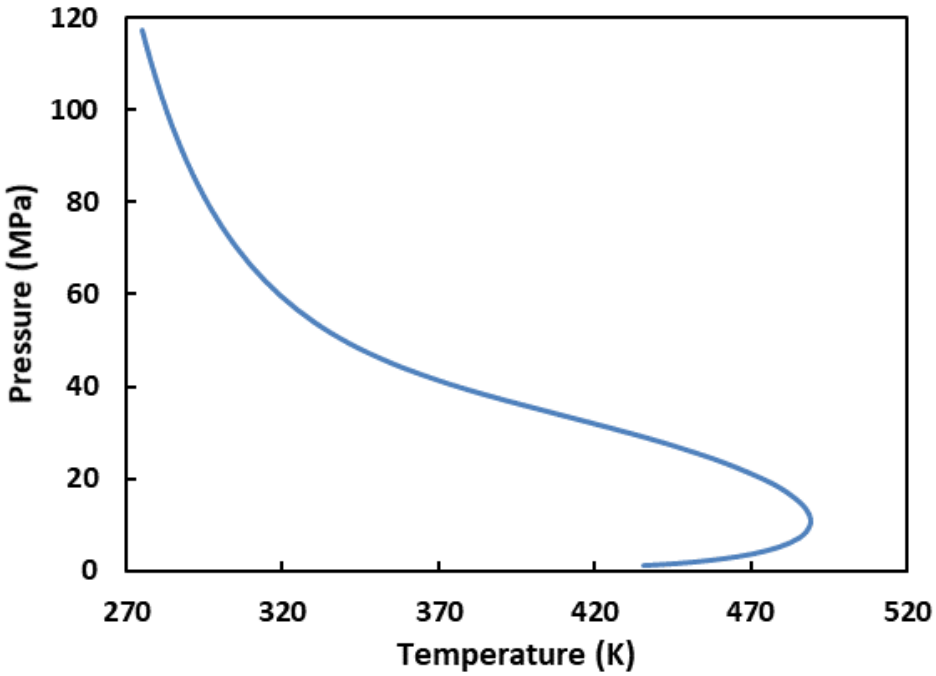

Figure 3.3: Phase envelop of the heavy gas

3.3 Schematic Representation of the Dynamic Plunger Lift Model in OLGA

The surface flow line and control valves along with the control schematics are considered in the dynamic simulation. As shown in Figure 3.4, both the motor valve and plunger activationsare setup with required time intervals in OLGA. For motor valve control, the time-series data in terms of open and close with time are given in the valve control configuration. As for the plunger, the launch time is required to simulate the plunger lift cycle. Furthermore, valve control and plunger control schematics should conform to perform successful simulations. In this simulation, the valve open time is 1 second earlier than the plunger launch time to ensure that the simulation runs successfully. The downstream surface line, valve, and separator are also incorporated in OLGA, but not in the proposed plunger lift model. According to the properly assumed boundary conditions, the length of the surface line, and the opening of the surface valve can be calculated.

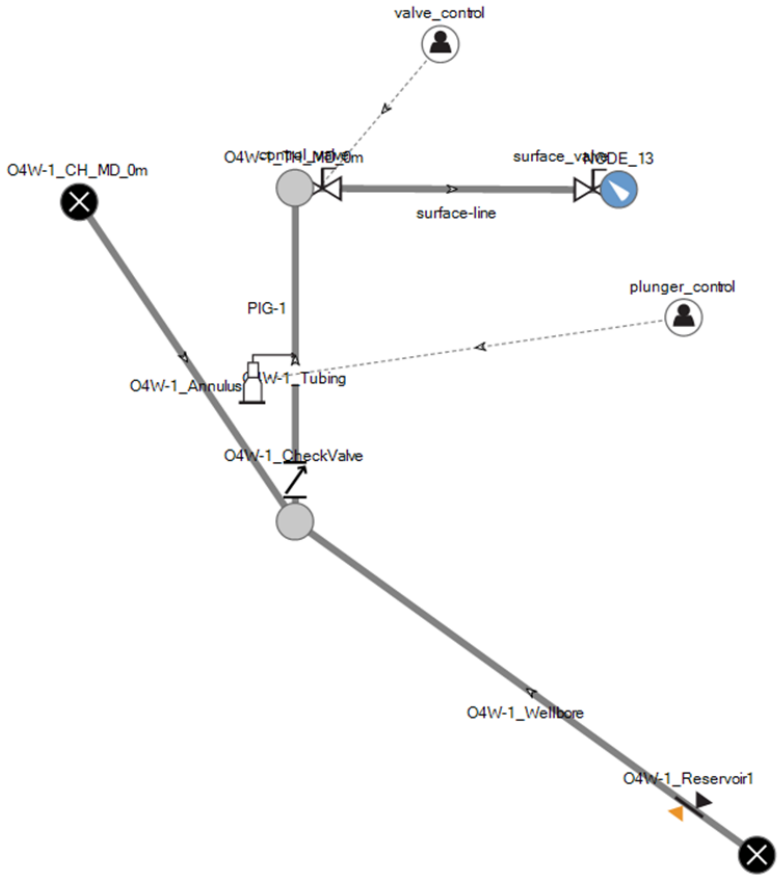

Figure 3.4: Schematic representation of the dynamic plunger lift model in OLGA

CHAPTER 4

SIMULATION RESULTS AND DISCUSSIONS

4.1 Plunger Lift Model Simulation for Single Cycle

Light gas with 93% methane mentioned in the previous section is used in the proposed model. All the parameters of the wellbore geometry, plunger, and reservoir are the same as the vertical well mentioned above. The initial casing pressure is 1.62 MPa and tubing pressure is 1.5 MPa. The line pressure is 1.1 MPa, which is the atmospheric pressure.

The calculation results from the proposed plunger lift model are presented and discussed in this section. The plunger lift model prediction includes pressure, plunger velocity, plunger acceleration, water heading, and gas production. When the valve opens, the simulation begins and the plunger is launched from the bottom of the well. The calculation time is 1600 seconds, which is a single plunger lift cycle.

4.1.1 Plunger Acceleration in Single Plunger Lift Cycle

Figure 4.1 presents the plunger acceleration in a single plunger cycle. As can be seen, at the very beginning, the plunger is pushed by the pressure below and accelerates sharply. However, the acceleration curve is not smooth. Both positive and negative values can be observed in the figure, which shows that the plunger can not only be accelerated but also decelerated due to the drag force from the slug and tubing wall. With the increase of the tubing roughness, the plunger can be decelerated obviously, which leads to a longer plunger movement time. Moreover, another

abrupt increase of the plunger acceleration occurs when the slug arrives at the surface due to the discharge of the liquid.

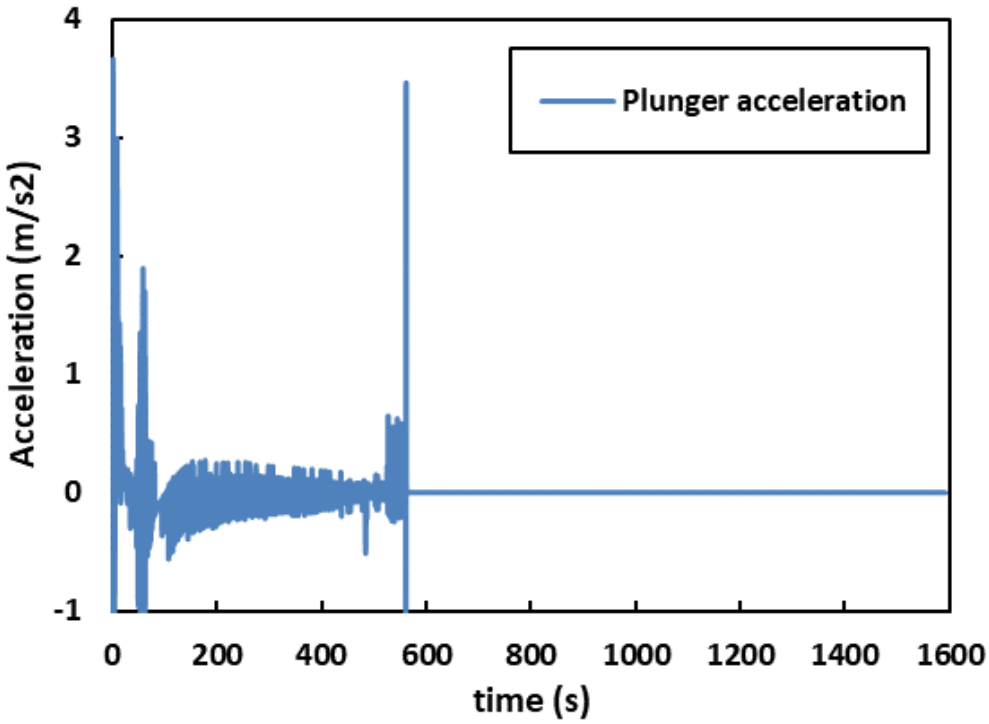

Figure 4.1: Plunger acceleration in single plunger lift cycle

4.1.2 Plunger Velocity in a Single Plunger Lift Cycle

Figure 4.2 shows the plunger velocity in a single plunger lift cycle. The plunger moves upward with a positive velocity and downward with a negative one. The plunger moves upward with a positive acceleration when the valve opens and its velocity increases sharply. After a few seconds, the plunger begins to decelerate due to the drag force. When a second peak appears, the plunger arrives at the surface and the slug is discharged from the tubing. Since the length of the liquid slug is much less than the wellbore depth, the acceleration period is very short. After the slug is discharged from the tubing, the plunger is caught by the lubricator and remains at the top

of tubing due to the high gas pressure in the tubing. During the gas blowout stage, the velocity of the plunger keeps zero. When the gas flow rate is not enough, the valve closes and the plunger drops to the bottom. The velocity changes smoothly due to the change of the gas and liquid densities. Equation (95) indicates that the plunger falls faster in gas phase due to a low density. At last, the plunger drops to the bottom of the tubing and sits on the bumper string.

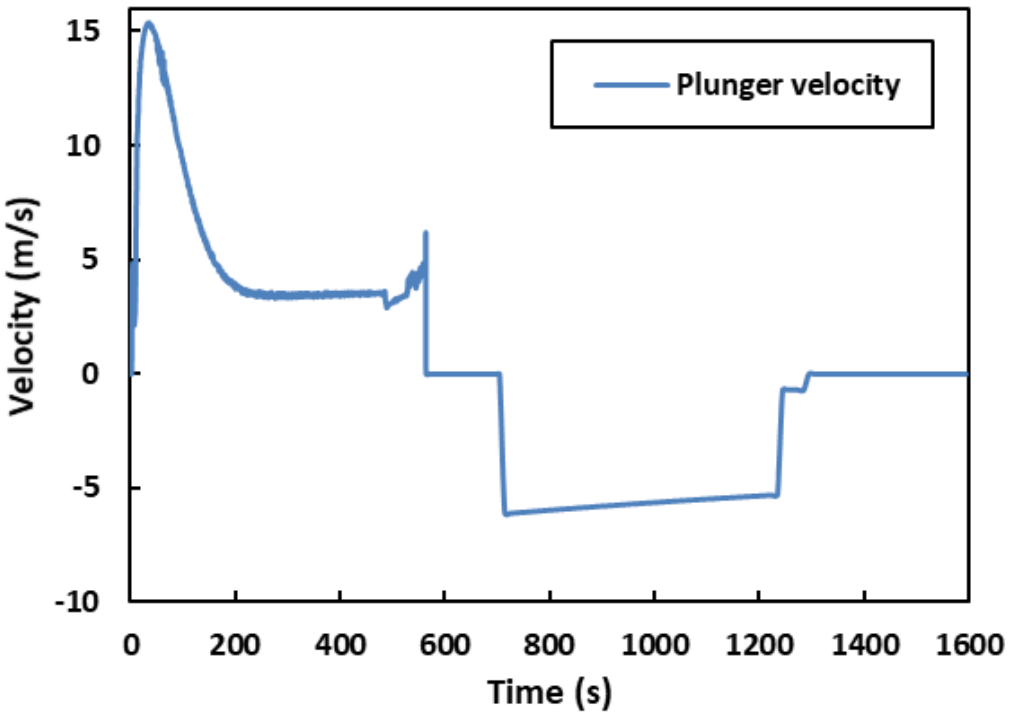

Figure 4.2: Plunger velocity in single plunger lift cycle

4.1.3 Production Rate in Single Plunger Lift Cycle

Figure 4.3 illustrates the gas production rate in a single plunger lift cycle. When the surface valve opens, the gas production rate surges to a very high level (2300 dm^3). After a few seconds, it decreases to a relative low level (500 dm^3). Since the fluid communication through the plunger is blocked by the liquid slug, the gas production rate decreases gradually when the plunger moves

upward. When the plunger arrives at the surface, another peak of gas production occurs since the slug is discharged and the gas below the plunger blows out. Later on, the gas production rate decreases to zero after the surface valve closes.

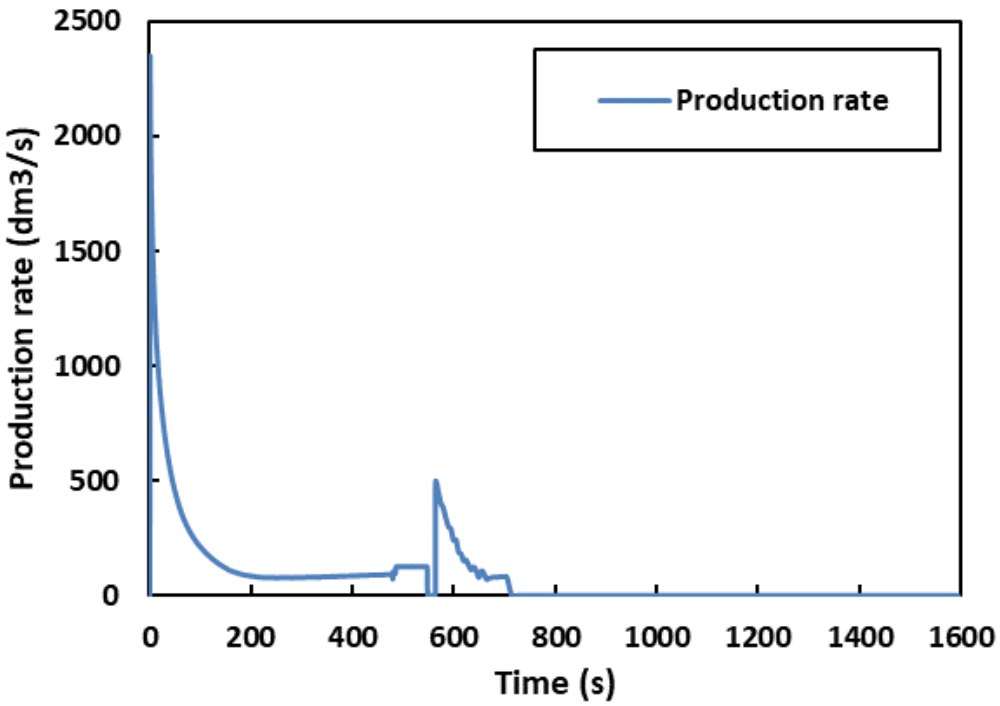

Figure 4.3: Production rate in single plunger lift cycle

4.1.4 Pressure in Single Plunger Lift Cycle

Figure 4.4 shows the tubing, casing, bottom hole and surface line pressure change versus time. The boundary condition shown by the red line is the surface line pressure, which equals to the atmospheric pressure. Both bottom hole pressure and casing pressure, which have a similar trend, decrease when the surface valve opens and increase when it closes. Tubing pressure drops quickly at the beginning when the surface valve opens. Then, a small peak of the tubing pressure occurs around 500 s, rising from 1.1 MPa to 1.2 MPa, when liquid slug reaches the surface. It

drops to the same value as the flow line pressure during the gas blowout stage. The build-up stage starts when the surface valve closes, after which the tubing pressure increases gradually.

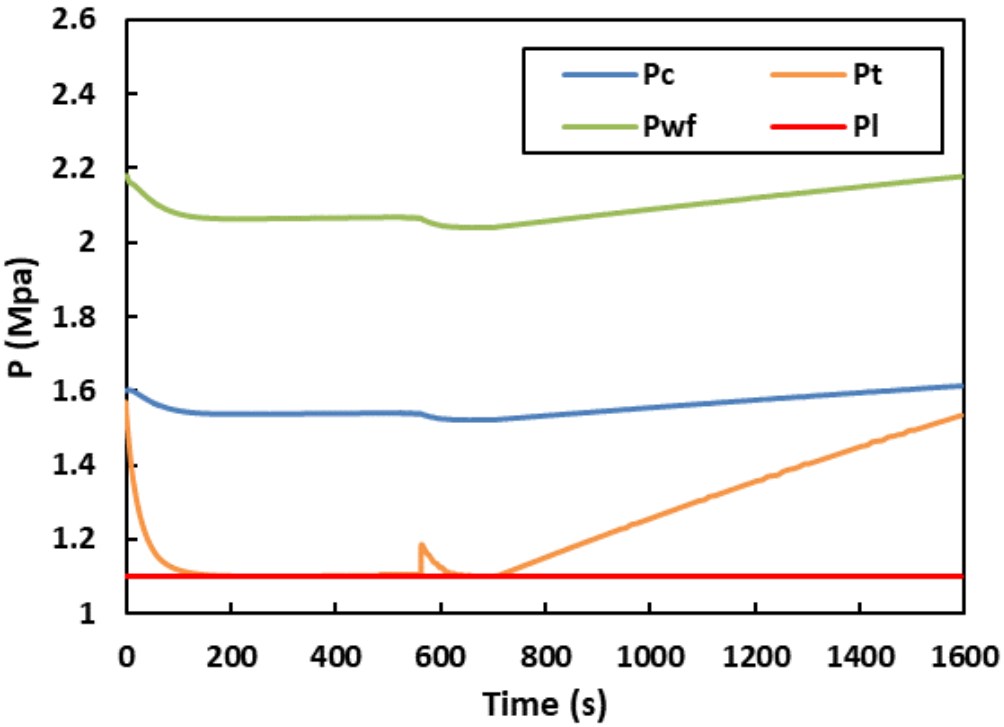

Figure 4.4: Pressure in single plunger lift cycle

4.1.5 Liquid Level in Single Plunger Lift Cycle

Figure 4.5 presents the liquid level in a single plunger lift cycle. Initially, the difference between the liquid levels of tubing and annulus is relatively small since the tubing pressure is close to that of the casing. When the plunger moves upward, the tubing pressure drops quickly while casing pressure is kept at 1.6 MPa. As a result, the liquid level difference increases rapidly. Later on, the plunger drops back to the bumper string and the build-up stage begins after the surface valve closes. Then, the liquid level in the tubing decreases gradually. As can be seen in Figure 4.5,

the tubing always has a longer liquid column in a plunger lift cycle, which shows an efficient liquid unloading process.

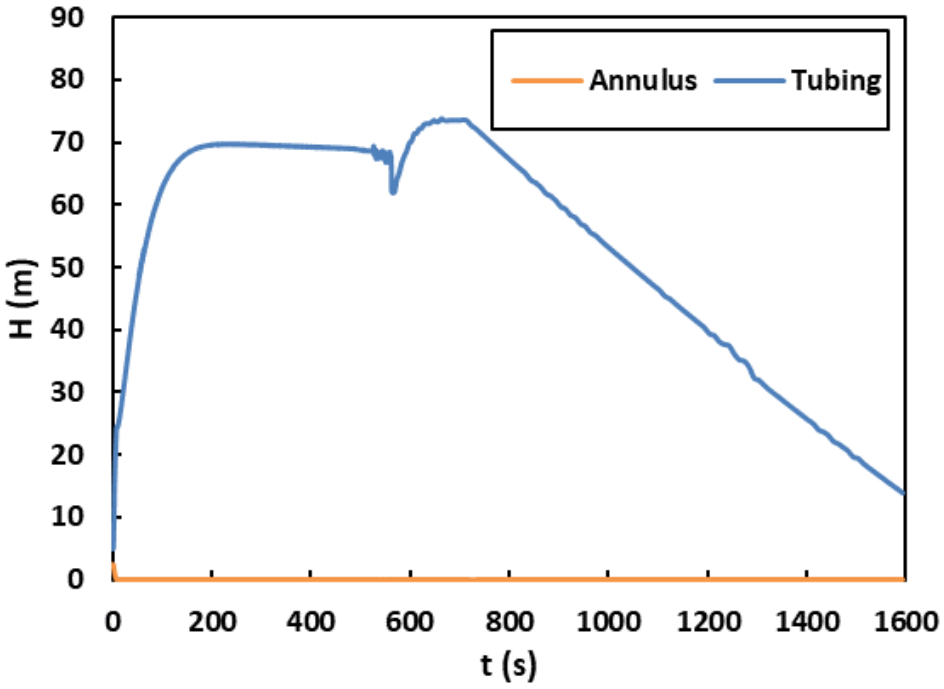

Figure 4.5: Liquid level in single plunger lift cycle

4.2 Abnormal Cases of the Plunger Lift Model

Success in plunger lift systems depends on proper candidate identification, proper well installation, and the effectiveness of the operator, all of which can contribute to the plunger lift problems. In this section, specific parameters will be applied to the mechanistic models or dynamic simulators to simulate anomalous patterns and failure events. Two examples of plunger lift anomalies are presented, including insufficient build-up time and liquid loading caused by a high water-gas ratio (WGR).

4.2.1 Insufficient Build-up Time

As the surface valve closes and plunger falls back to the bumper string, the gas blowout stage ends, and the tubing pressure reaches the minimum. After the build-up stage, the wellbore achieves enough pressure and energy to push the plunger and liquid slug to the surface. However, if the build-up time is too short that cannot supply enough tubing pressure, the plunger will stop during the ascent and fall back to the bottom of the well. Then, the liquid slug cannot be discharged in this plunger lift cycle. As shown in Figure 4.6, the well is closed at 600 s and reopened at 1200 s after the first plunger lift cycle. The tubing pressure only reached 1.4 MPa. Figure 4.7 shows that there is no second peak of gas production rate in the second plunger lift cycle, which indicates that the plunger fails to push the liquid slug to the surface. Figure 4.8 shows that there is still a 30 m liquid column that stays in the tubing when the valve is opened at 1200 s, which indicates that the tubing does not have enough energy to push the liquid slug to the surface. When the plunger reachs the bumper spring, the tubing pressure sharply increases to over 1.3 MPa since the liquid slug falls back with the plunger.

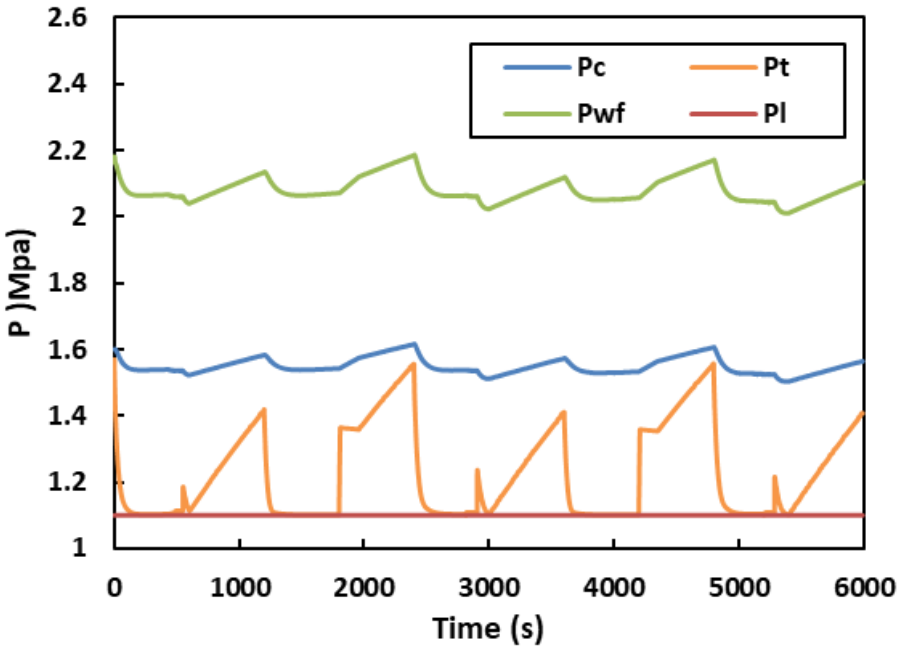

Figure 4.6: Pressure in multiple plunger lift cycles for insufficient build-up time

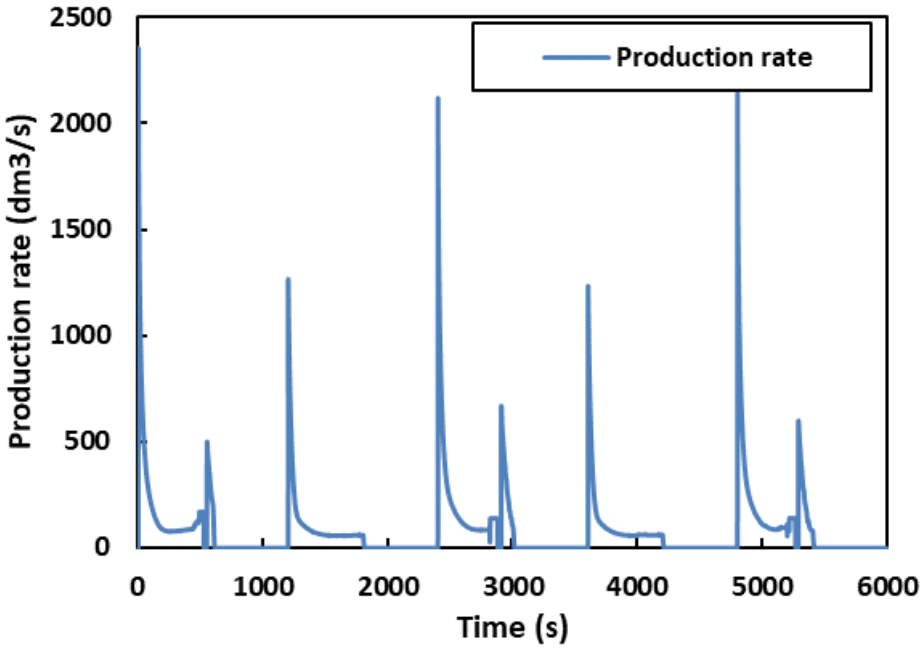

Figure 4.7: Production in multiple plunger lift cycles for insufficient build-up time

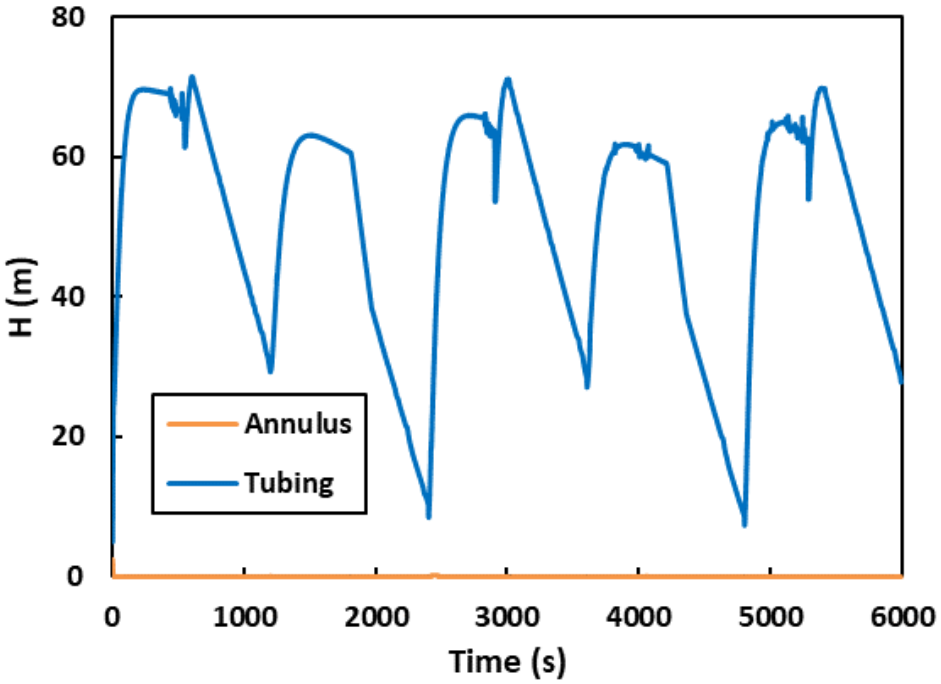

Figure 4.8: Liquid level in multiple plunger lift cycles for insufficient build-up time

4.2.2 Liquid Loading Caused by High Water Gas Ratio (WGR)

Liquid loading in a gas well is the inability of the produced gas to lift the produced liquids from the wellbore. Under this condition, produced liquid accumulates in the wellbore leading to a reduced production rate till the well can no longer produce. With the liquid level increase in the gas well as shown in Figure 4.10, the difference between casing pressure and tubing pressure becomes larger in Figure 4.9.

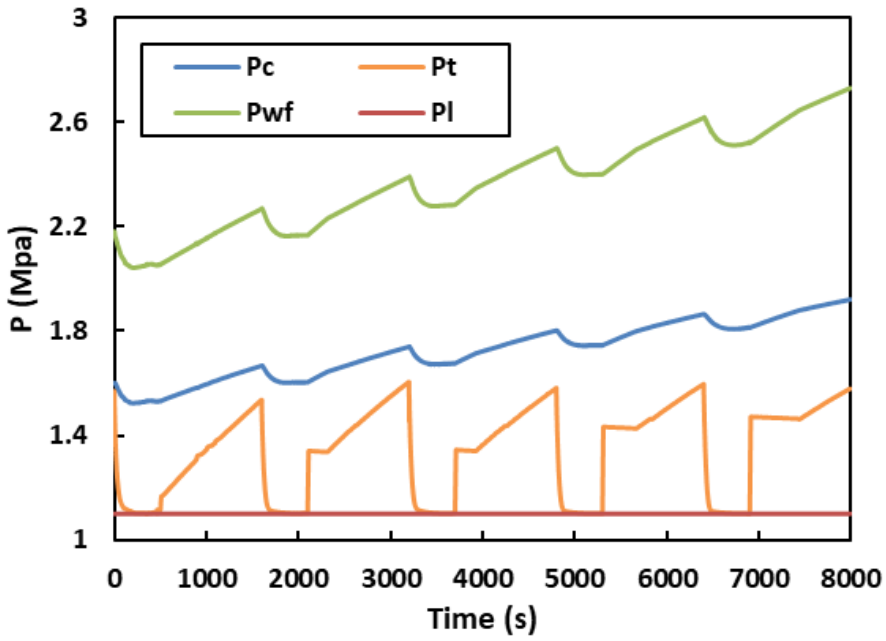

Figure 4.9: Pressure in multiple plunger lift cycles for liquid loading

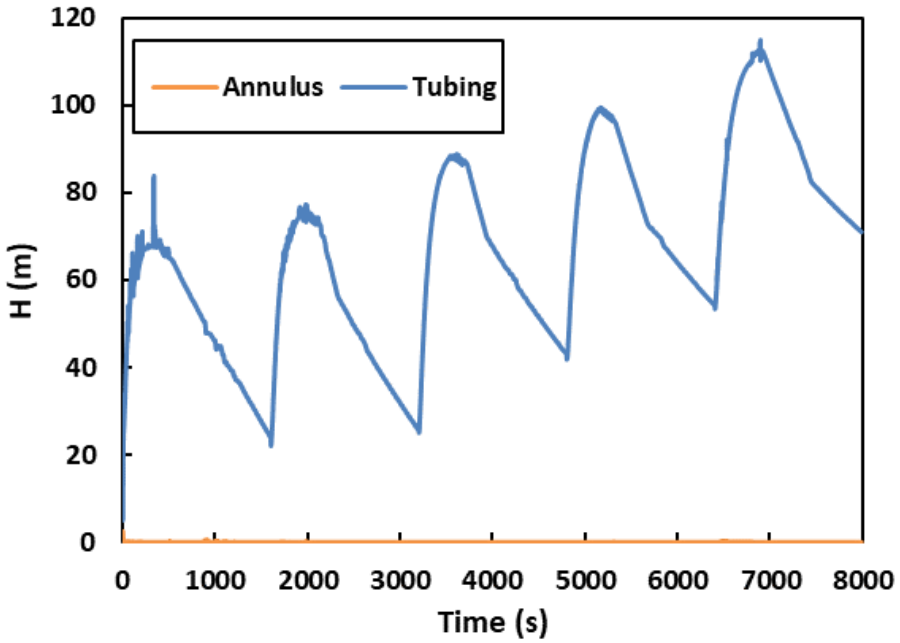

Figure 4.10: Liquid level in multiple plunger lift cycles for liquid loading

4.3 Comparisons between Compositional Model and Black-Oil Model

Fluid properties can be calculated with the compositional model and black-oil model. Applying different models can achieve different results. The compositional model is recommended for light oils, condensates, and natural gas, while the black-oil model is suggested for non-volatile oils since it assumes that the composition of the oil and gas do not change with pressure and temperature. In this section, two methods are compared and analyzed for different gas mixtures using the new model and OLGA simulation.

4.3.1 Light Gas Case

Table 4.1: The composition for light gas

Component	**Mol %**
N2	0.13
CO2	0.18
C1	93.00
C2	6.69

As shown in Table 4.1, the light gas is the same as that used in Section 3.2 OLGA simulation. According to the gas composition, the relative gas density of the black-oil model is 0.6. A slight difference can be captured using the compositional model and black-oil model in Figure 4.11. Since the plunger is not sealed by a liquid slug in the valve opening stage, there is no difference between the two models. When the surface valve is closed, the tubing pressure calculated by the compositional model is slightly lower than that by the black-oil model.

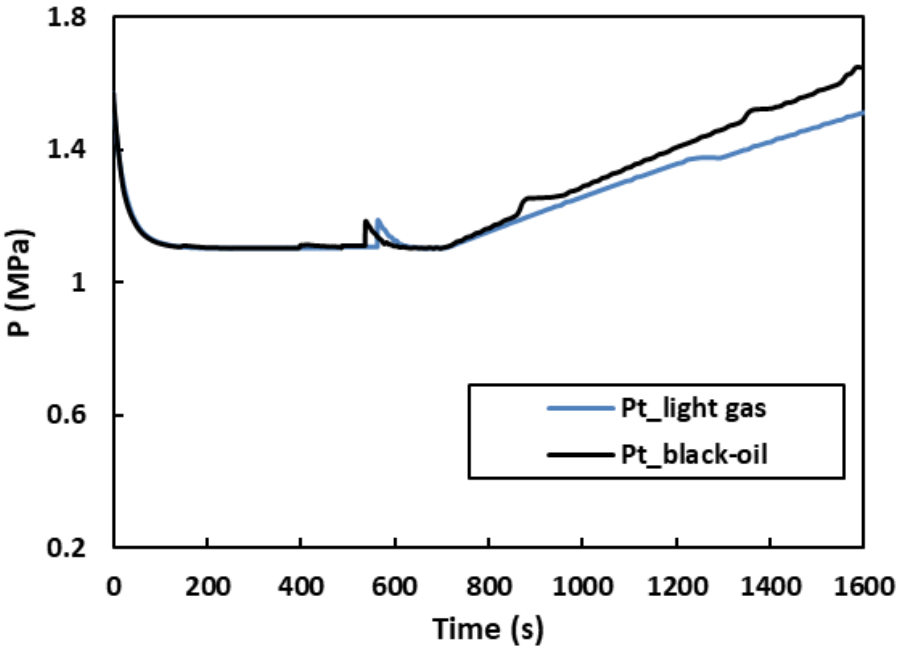

Figure 4.11: Tubing pressure of the compositional model and black-oil model for light gas

Figure 4.12 shows the casing pressures using the compositional model and black-oil model. When the slug is discharged from the tubing string, the casing pressure of the compositional model is slightly higher than that of the black-oil model, which agrees with the less produced gas by the black-oil model shown in Figure 4.13. The difference in the pressure is only 0.008 MPa, 0.5% of the casing pressure. Therefore, the results of the compositional model and black-oil model are similar when all of the gas components are in the vapor phase.

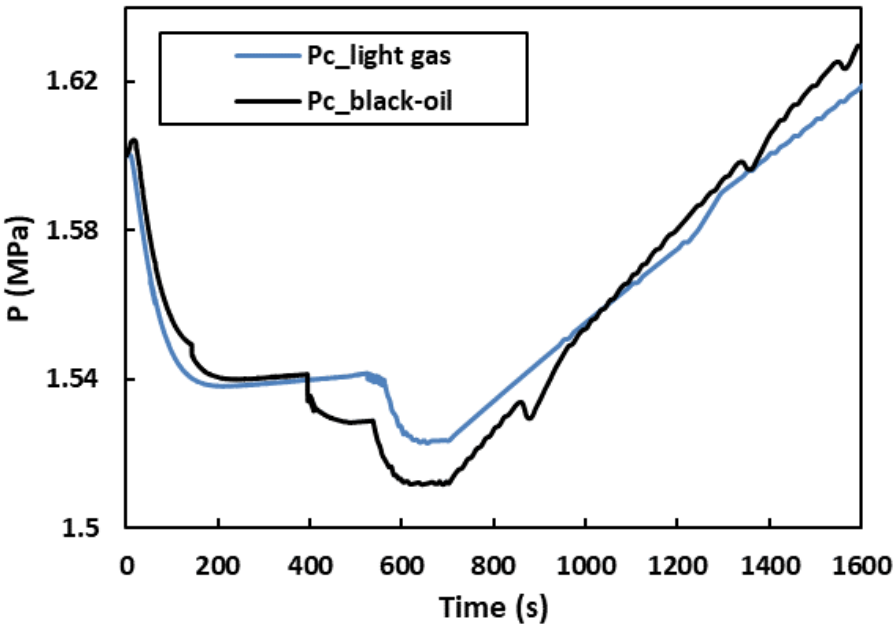

Figure 4.12: Casing pressure of the compositional model and black-oil model for light gas

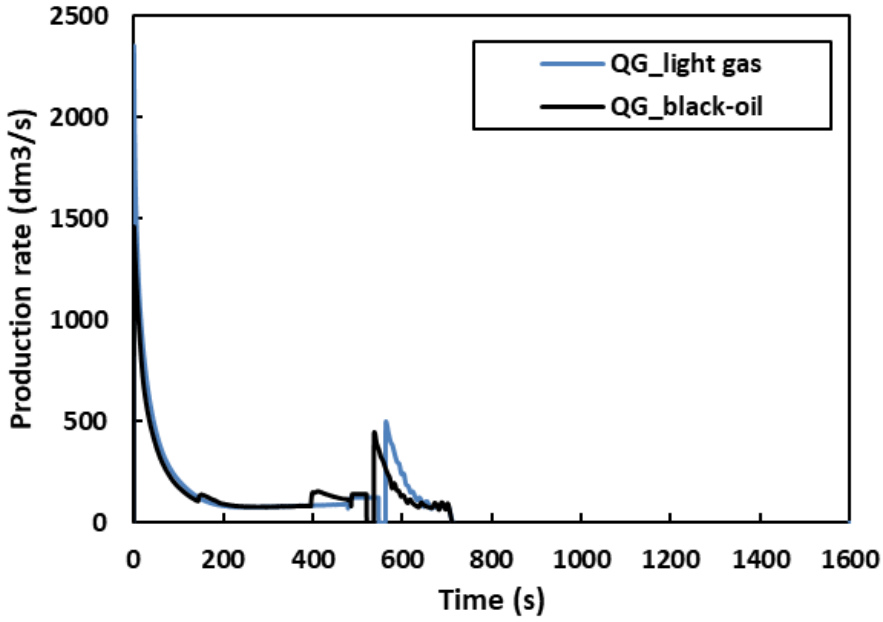

Figure 4.13: Gas production of the compositional model and black-oil model for light gas

Since the casing pressure is above the bubble point, oil and gas phases maintain a fixed-composition throughout the process simulated in the reservoir. As a result, the black-oil model is valid throughout the simulation. Under similar conditions, all the properties are a function of pressure and the compositional model can be replaced by the black-oil model.

4.3.2 Gas-Condensate Case

Similarly, the gas listed in Table 4.2 has the same composition as the heavy gas used in OLGA simulation, in which some heavy gas components are included. The pressure and gas production rate of the plunger lift model using the compositional model and black-oil model are presented in this section.

Table 4.2: The composition for heavy gas

Component	**Mol %**
CO2	0.18
C1	61.92
C2	14.08
C3	8.35
iC4	0.97
nC4	3.41
iC5	0.84
nC5	1.48
C6	1.79
C7+	6.85

The specific gravity of the black-oil model is 1.2, which is the same as that from the compositional model. Different from the light gas, the results of the compositional model and black-oil model show an obvious difference in casing pressure and gas production. As shown in Figure 4.14, the compositional model and black-oil model shows a similar trend and values in tubing pressure. However, Figure 4.15 shows a different trend when the surface valve opens. At 150 s, casing pressure calculated by the compositional model drops much more quickly than that by the black-oil model. The maximum difference of casing pressure between the compositional model and black-oil model is 0.04 MPa, which is 2.5% of the total casing pressure. Moreover, the plunger velocity of the compositional model is faster than that of the black-oil model. As shown in Figure 4.16, the second peak of the gas production for the compositional model is more than a hundred seconds earlier.

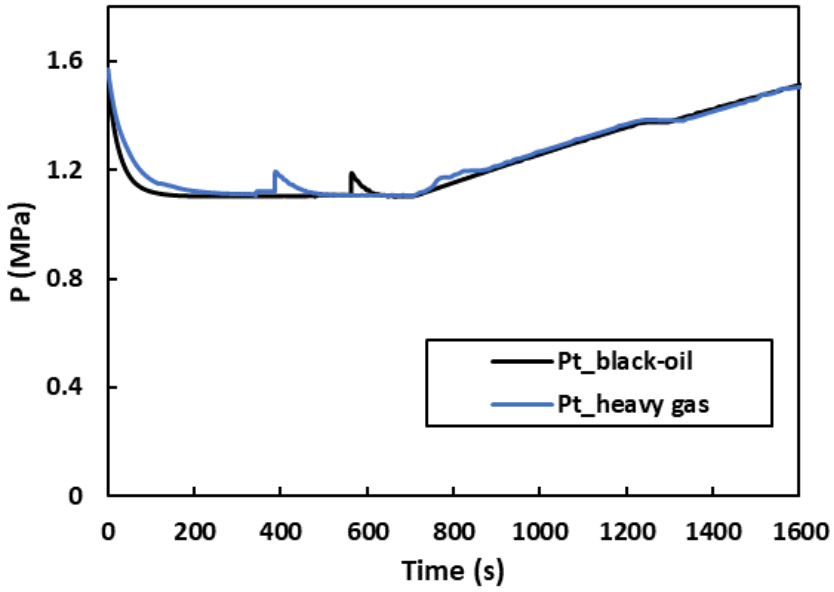

Figure 4.14: Tubing pressure of the compositional model and black-oil model for heavy gas

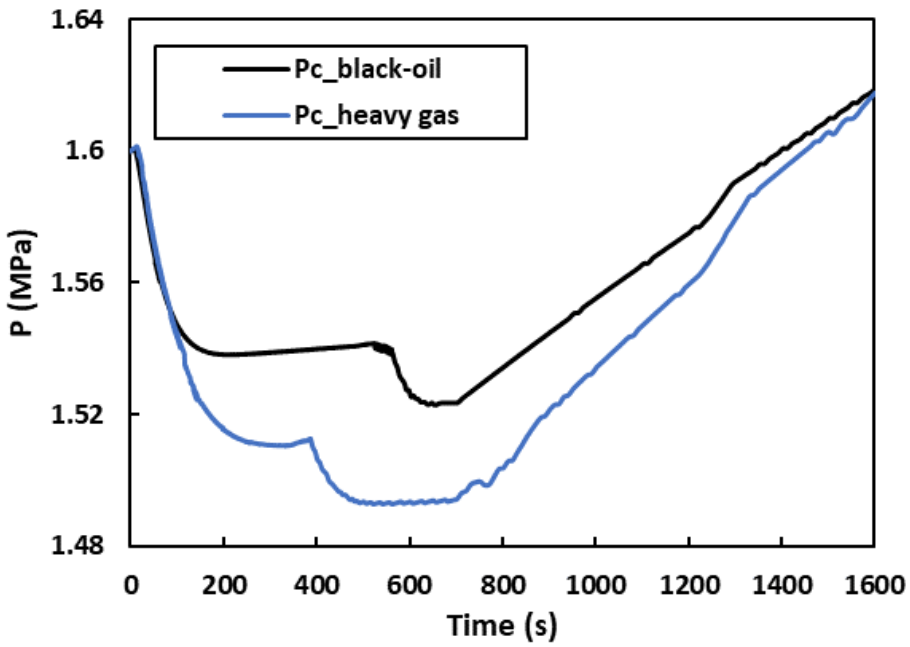

Figure 4.15: Casing pressure of the compositional model and black-oil model for heavy oil

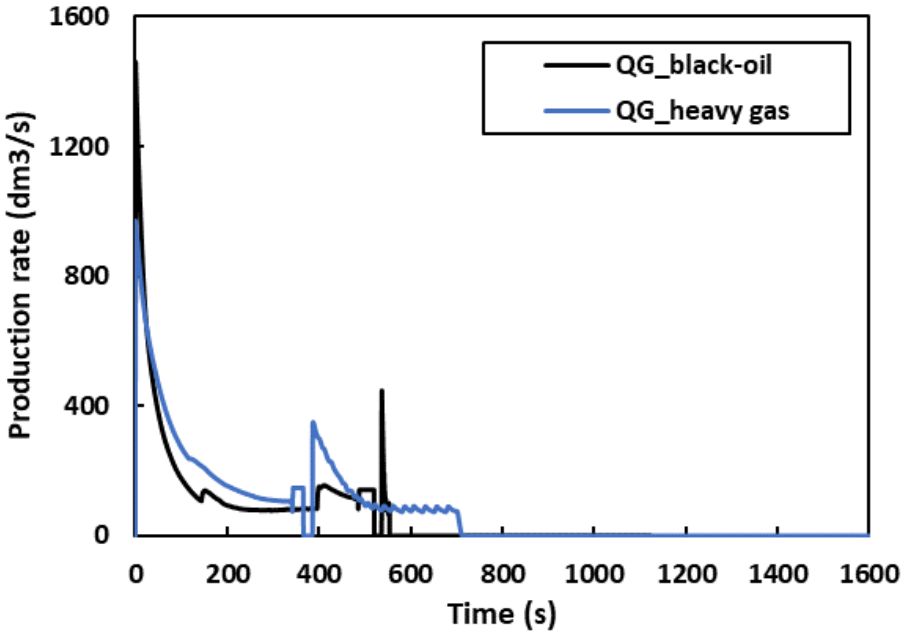

Figure 4.16: Gas production of the compositional model and black-oil model for heavy gas

4.4 OLGA Simulation Results

In this section, the OLGA simulation results are presented and compared to those calculated by the new model of this study. Fluid properties and wellbore geometry are given in Chapter 3. Light gas and gas condensate simulations are conducted.

4.4.1 Light Gas Case

As shown in Figure 4.17, the change of the tubing pressure has a similar trend between OLGA simulation and the new plunger lift model. For the casing pressure, Figure 4.18 shows a different trend between the OLGA model and the new plunger lift model simulation. That is due to the blockage of a plunger, where the liquid slug stops the communication of fluids through the plunger. In reality, the liquid slug leaks though the clearance between the plunger and tubing wall. The pressure drops from the two simulations are close, about 0.08 MPa.

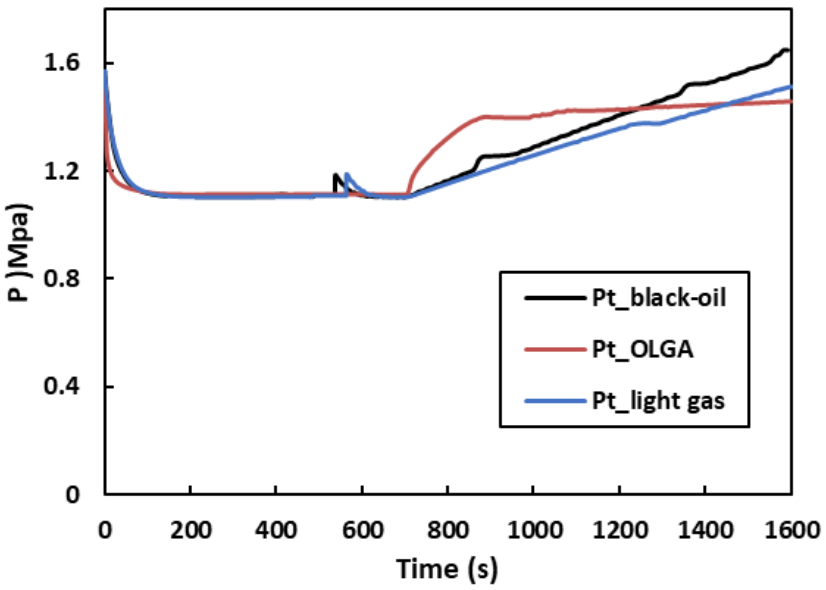

Figure 4.17: Tubing pressures of OLGA and new plunger lift model simulations for light gas

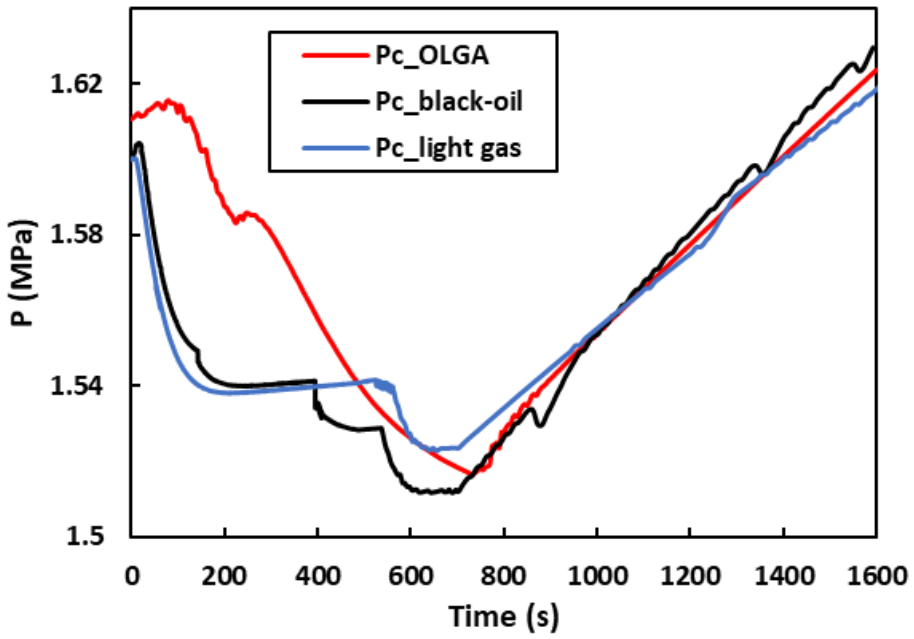

Figure 4.18: Casing pressures of OLGA and new plunger lift model simulations for light gas

Compared to OLGA simulation for light gas, both the black-oil model and compositional model can make a good prediction by the new model. However, more details need to be included in the future work, for example, the liquid leakage through the plunger. Considering the computational cost, the black-oil model is recommended for light gas cases.

4.4.2 Gas Condensate Case

Figure 4.19 shows the tubing pressures calculated by the OLGA model and the new model, respectively. As shown in Figure 4.20, the casing pressure drop of the OLGA simulation is different from that calculated by the black-oil model using the new simulator. The pressure drop of OLGA simulation is about 0.1 MPa, larger than that of the black-oil model (0.07 MPa). On the contrary, the pressure drop calculated by the compositional model has a similar trend with that of

OLGA simulation since the gas composition changes throughout the plunger lift cycle. Therefore, it is recommended to use the compositional model for a heavy gas simulation.

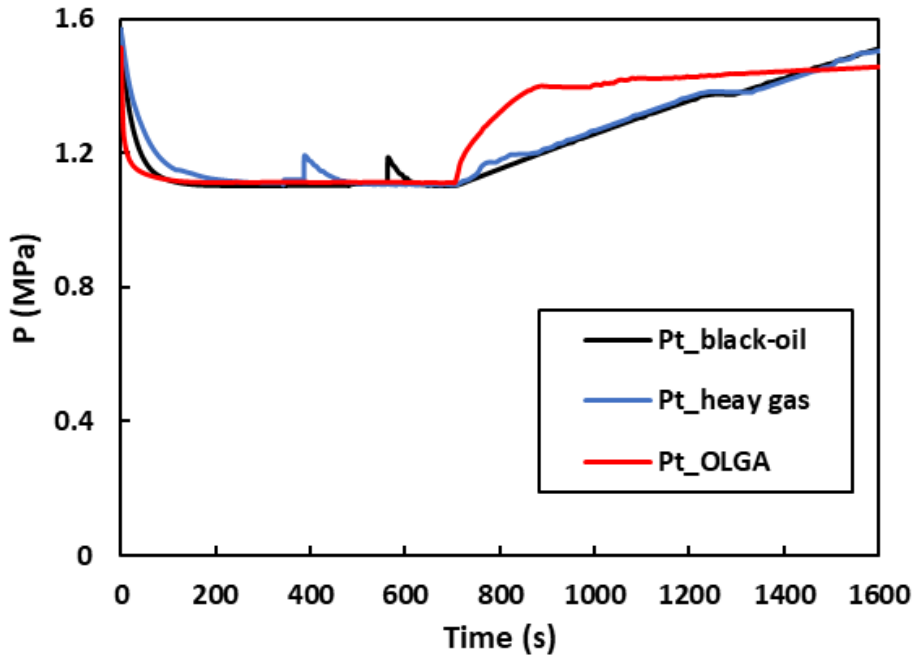

Figure 4.19: Tubing pressures of OLGA and new plunger lift model simulations for gas condensate

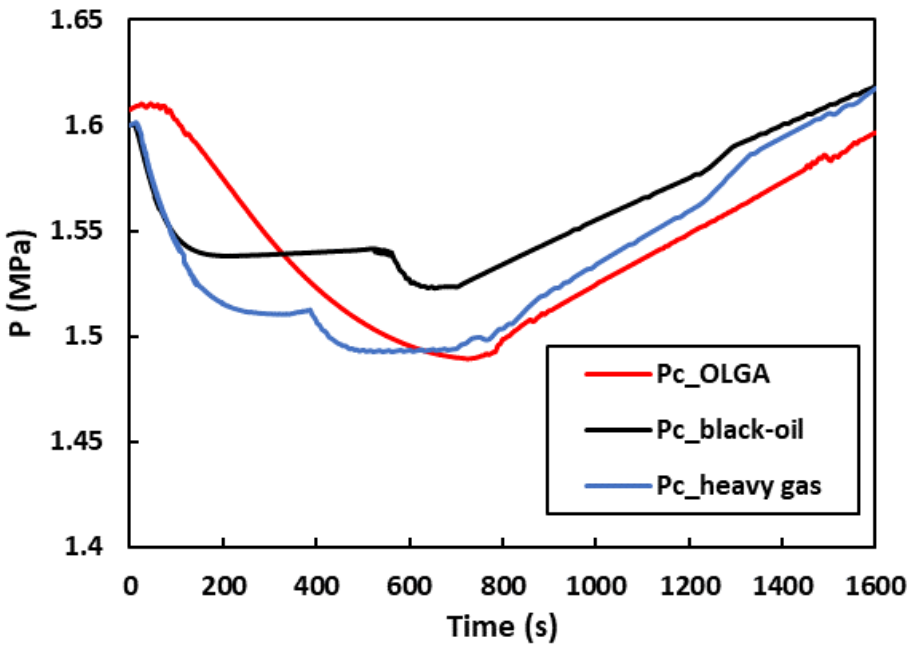

Figure 4.20: Casing pressures of OLGA and new plunger lift model simulations for gas condensate

For a heavy gas mixture, the fixed gas and oil compositions in the black-oil model is no longer valid. In reservoirs that contain light oil, for example, gas condensate and volatile oils, the fluid properties and vapor/liquid equilibrium depend on fluid composition, pressure, and temperature. More complex fluid behavior requires all hydrocarbon phases to be considered as mixtures of normal components. Therefore, the "composition simulation" equilibrium flash calculation using *K* value or EOS must be incorporated. Many condensate fluids exhibit retrograde condensation, which occurs along with the pressure reduction. This abnormal behavior can be observed within the two-phase envelope between the critical point. As a result, the phase behavior can only be calculated through a variable compositional model for volatile oils and condensate fluids.

CHAPTER 5

CONCLUSIONS AND RECOMMENDATIONS

5.1 Summary and Conclusions

The following conclusions are made after analyzing and comparing the new plunger lift model predictions with OLGA simulations:

1. The new plunger lift model for the liquid unloading process is developed based on Gasbarri and Wiggins's (2001) dynamic model and Gupta et al. (2017) plunger lift modeling framework.
2. Comparing to previous models, plunger velocity equations, reservoir performances, and a flash model are incorporated into the new model, which provides more accurate and reasonable predictions.
3. Instead of using the constant plunger falling velocities in the tubing, the new model calculates plunger falling velocity in the downstroke phase based on plunger gravity and drag force.
4. The presented model restricts the unreasonable prediction of gas flow rate above the plunger in the upstroke phase within the gas flow rate corresponding to the local sound speed.
5. According to the predictions by OLGA and the new model, the phase behavior of volatile oils and condensate fluids can be accurately calculated by a variable composition model. Considering the computational cost, the black-oil model is more suitable for dry gas.

5.2 Recommendations

1. Liquid leakage through the clearance between the plunger and tubing wall, liquid slug discharge dynamics, and the multiphase flow behavior below the plunger needs to be included in the future work.
2. More complex well trajectory, especially deviated well trajectory needs to be included in the new plunger lift model.
3. In this study, the equations of state (EOS) of the compositional model is Peng-Robinson (PR). Other EOS models including but not limited to van der Waals, Redich-Kwong (RK), Soave-Redlich-Kwong (SRK) may be incorporated for different cases.

NOMENCLATURE

A	area, m^2 or constant number
a	acceleration, m/s^2
B	constant
b	denotation
C	constant
C_{res}	reservoir flow constant
C_v	flow coefficient, $kg/s \cdot Pa^{-0.5}$
C_d	drag coefficient
D *or* d	diameter, m
F	mass flow rate, kg/s
g	gravitational acceleration, m/s^2
GLR	gas-liquid ratio, m^3/ m^3
H	depth, m
L	length, m
M	molecular weight, kg/mol
m	mass, kg
P	pressure, Pa
q	volumetric flow rate, m^3/s
R	gas constant, J/mol/K or radius, m

Re	Reynolds number
T	temperature, K
t	time, s
V	velocity, m/s
w	weight, kg
Z	compressibility

Greek Letters

α	denotation
ε	wall roughness, m
ρ	density, kg/m^3
μ	viscosity, Pa·s

Subscripts

1	control volume in
2	control volume out
a or ann	annulus
b	bottom
c	casing
fric	friction
g	gas
l	liquid or production line
out	out
p	plunger
res	reservoir

s	slug
SC or std	standard condition
t or tub	top or tubing
tt	tubing top
tb	tubing bottom
w	wellbore
wf	well flowing

BIBLIOGRAPHY

Avery, D.J. and Evans, R.D. (1988). Design optimization of plunger lift systems. Proceedings of SPE AIME conference: International Meeting on Petroleum Engineering. Tianjin, China, November 1-4, 1988: Paper No. SPE-17585-MS.

Brill, J.P., Mukherjee, H. (1999). Multiphase Flow in Well. Monograph Series, Society of Petroleum Engineers, Richardson, Texas, USA. http://doi.org/10.2118/16242-PA

Gupta, A., Kaisare, N. S. and Nandola, N. N. (2017). Dynamic plunger lift model for deliquification of shale gas wells. Computers and Chemical Engineering, 103, 81-90. https://doi.grg/10.1016/j.compchemeng.2017.03.005

Hashmi, G. M., Hasan, A. R. and Kabir, C. S. (2016). Design of plunger lift for gas wells. Proceedings of SPE North America Artificial Lift Conference and Exhibition, The Woodlands, Texas, USA,25-27 October, 2016: Paper No. SPE-181220-MS.

Kannan, S. K., Matthew, B., Ge, Yuan., Haidan, L. and Ghislain, F. (2019). Modeling and optimization of gas-assisted plunger lift GAPl by a transient simulator: A case study of a permian shale well. Proceedings of SPE Eastern Regional Meeting, Charleston, West Virginia, USA, 15-17 October, 2019: Paper No. SPE-196581-MS.

LEA, J. F. (1982). Dynamic Analysis of Plunger Lift Operations. Journal of Petroleum Engineers, 34, 2617-2629. http://doi.org/10.2118/10253-PA

Li, Z., Ripepi, N. and Chen, C. (2019). Comprehensive laboratory investigation and model fitting of Klinkenberg Effect and its role on apparent permeability in various U.S. shale formations. Proceedings of 53rd U.S. Rock Mechanics/Geomechanics Symposium. New

York City, New York, 23-26 June, 2019: Paper No. ARMA-2019-1568.

Li, Z., Ripepi, N. and Chen, C. (2020). Using pressure pulse decay experiments and a novel multi-physics shale transport model to study the role of Klinkenberg effect and effective stress on the apparent permeability of shales. Journal of Petroleum Science and Engineering, 189, 107010. http://doi.org/10.1016/j.petrol.2020.107010

Maggard, J. B., Wattenbarger, R. A. and Scott, S. L. (2000). Modeling plunger lift for water removal from tight gas wells. Proceedings of the SPE Gas Technology Symposium. Calgary Alberta, Canada, 3-5 Apirl: Paper No. SPE-59747-MS

Marcano, L. and Chacin, J. (1994). Mechanistic design of conventional plunger-lift installation. SPE Advanced Technology Series, 2, 15–24. http://doi.org/10.2118/23682-PA

Mohan, K. (2008). Natural Gas Engineering. PennWell, Tulsa, Oklahoma, USA.

Nandola, N. N., Kaisare, N. S. and Gupta, A. (2018). Online optimization for a plunger lift process in shale gas wells. Computers and Chemical Engineering. http://doi.org/10.1016/j.compchemeng.2017.09.001

Nguyen, H. T. and Mundo, F. C. Del (2016). Improving Artificial Lift Design Through Dynamic Simulation, 108, 89-97. Proceedings of the SPE North America Artificial Lift Conference and Exhibition, The Woodland, Texas, USA, 25-27 October, 2016: Paper No. SPE-181243-MS.

Rowlan, O, L., Rick, N., Carolyn, C., James, F, L. and James, N, M. (2013). Measured plunger fall velocity used to calibrate new fall velocity model. Proceedings of the SPE Production and Operations Symposium. Oklahoma City, Oklahoma, USA, 23-26, March, 2013: Paper No. SPE-164495-MS

Tang, Y., Tang, Y., Li, Z., Wang, R., Cui, M., Wang, X., Lun, Z. and Lu, Y. (2019).

Experimental Study on the Density-Driven Carbon Dioxide Convective Diffusion in Formation Water at Reservoir Conditions. Proceedings of the American Chemical Society Omega, 4, 11082-11092. https:// doi.org/10.1021/acsomega.9b00627

Veeken, C. and Al Kharusi, D. (2019). Selecting artificial lift or deliquification measures for deep gas wells in the sultanate of Oman. Proceedings of the Society of Petroleum Engineers - SPE Kuwait Oil and Gas Show and Conference 2019, KOGS 2019. Mishref, Kuwait, 13-16, October, 2019: Paper No. SPE-198080-MS.

Zhu, H., Jianjun, Z., Rutter, R., Jiecheng, Z., & Zhang, H.-Q. (2018a). Sand Erosion Model Prediction, Selection and Comparison for Electrical Submersible Pump (ESP) using CFD Method. Proceedings of the ASME 2018 5th Joint US-European Fluids Engineering Division Summer Meeting. https://doi.org/10.1115/FEDSM2018-83179

Zhu, H., Zhang, J., Zhu, J., Rutter, R., & Zhang, H.-Q. (2019a). A Numerical Study of Turbulence Model and Rebound Model Effect on Erosion Simulations in an Electrical Submersible Pump (ESP). Proceedings of the ASME 2019 ASME-JSME-KSME Joint Fluids Engineering Conference. San Francisco, CA, USA, July 28-Aug 1: Paper No. AJKFLUIDS2019-5538. https://doi.org/10.1115/AJKFluids2019-5538

Zhu, H., Zhu, J., Rutter, R., & Zhang, H.-Q. (2019b). A Numerical Study on Erosion Model Selection and Effect of Pump Type and Sand Characters in Electrical Submersible Pumps (ESPs) by Sandy Flow. Journal of Energy Resources Technology, 141(12), 122004. https://doi.org/10.1115/1.4044941

Zhu, H., Zhu, J., Zhang, J., & Zhang, H. Q. (2017a). Efficiency and Critical Velocity Analysis of Gravitational Separator through CFD Simulation. Proceedings of the ASME International Mechanical Engineering Congress and Exposition, https://doi.org/10.1115/IMECE2017-

71230

Zhu, H., Zhu, J., Zhou, Z., Rutter, R., Forsberg, M., Gunter, S., & Zhang, H. Q. (2019c). Experimental Study of Sand Erosion in Multistage Electrical Submersible Pump ESP: Performance Degradation, Wear and Vibration. Proceedings of the SPE International Petroleum Technology Conference. https://doi.org/10.2523/IPTC-19264-MS

Zhu, H., Zhu, J., Zhou, Z., Rutter, R., & Zhang, H. Q. (2019d). Wear and Its Effect on Electrical Submersible Pump ESP Performance Degradation by Sandy Flow: Experiments and Modeling. Proceedings of the Offshore Technology Conference. https://doi.org/10.4043/29480-MS

Zhu, H. (2019). Experiments, CFD Simulation and Modeling of Sand Wear and Performance Degradation in ESPs. Ph.D. Disertation. University of Tulsa.

Zhu, J., Farfan, J. A. M., Zhang, J., Cuamatzi-Melendez, R., Zhu, H., & Zhang, H. Q. (2018b). Flow Pattern Prediction in Electrical Submersible Pump (ESP) under Gassy Flow Conditions using Transient Multiphase CFD Methods with Visualization Experimental Validation. Proceedings of the ASME 2018 5th Joint US-European Fluids Engineering Division Summer Meeting, https://doi.org/10.1115/FEDSM2018-83081

Zhu, J., Wang, Z., Zhu, H., Cuamatzi-Melendez, R., Martinez-Farfan, J. A., Jiecheng, Z., & Zhang, H. Q. (2018c). Mechanistic Modeling of Electrical Submersible Pump ESP Boosting Pressure under Gassy Flow Conditions and Experimental Validation. Proceedings of the SPE Annual Technical Conference and Exhibition.

Zhu, J., Zhang, J., Cao, G., Zhao, Q., Peng, J., Zhu, H., & Zhang, H. Q. (2019e). Modeling Flow Pattern Transitions in Electrical Submersible Pump under Gassy Flow Conditions. Journal of Petroleum Science and Engineering, 180, 471–484.

https://doi.org/10.1016/j.petrol.2019.05.059

Zhu, J., Zhang, J., Zhu, H., & Zhang, H. Q. (2018d). A Mechanistic Model to Predict Flow Pattern Transitions in Electrical Submersible Pump under Gassy Flow Condition. Proceedings of the SPE Artificial Lift Conference and Exhibition. https://doi.org/10.2118/190927-MS

Zhu, J., Cao, G., Tian, W., Zhao, Q., Zhu, H., Song, J. , Peng, J., Lin, Z., Zhang, H.Q. (2019f). Improved Data Mining for Production Diagnosis of Gas Wells with Plunger Lift through Dynamic Simulations. Proceedings of SPE Annual Technical Conference and Exhibition. https://doi.org/10.2118/196201-MS

Zhu, J., Zhu, H., Cao, G., Banjar, H., Peng, J., Zhao, Q., & Zhang, H.-Q. (2019g). A New Mechanistic Model for Oil-Water Emulsion Rheology and Boosting Pressure Prediction in Electrical Submersible Pumps ESP. Proceedings of the SPE Annual Technical Conference and Exhibition. https://doi.org/10.2118/196155-MS

Zhu, J., Zhu, H., Zhao, Q., Fu, W., Shi, Y., & Zhang, H. Q. (2019h). A Transient Plunger Lift Model for Liquid Unloading from Gas Wells. Proceedings of SPE International Petroleum Technology Conference. https://doi.org/10.2523/19211-MS

Zhu, J., Zhu, H., Cao, G., Zhang, J., Peng, J., Banjar, H., & Zhang, H. Q. (2019i). A New Mechanistic Model to Predict Boosting Pressure of Electrical Submersible Pumps ESPs under High-Viscosity Fluid Flow with Validations by Experimental Data. Proceedings of the SPE Gulf Coast Section Electric Submersible Pumps Symposium. https://doi.org/10.2118/194384-MS

Zhu, J., Zhu, H., Wang, Z., Zhang, J., Cuamatzi-Melendez, R., Farfan, J. A. M., & Zhang, H. Q. (2018e). Surfactant Effect on Air/Water Flow in a Multistage Electrical Submersible Pump

(ESP). Experimental Thermal and Fluid Science, 98, 95–111. https://doi.org/10.1016/j.expthermflusci.2018.05.013

Zhu, J., Zhu, H., Zhang, J., & Zhang, H. Q. (2017b). An Experimental Study of Surfactant Effect on Gas Tolerance in Electrical Submersible Pump (ESP). Proceedings of the ASME International Mechanical Engineering Congress and Exposition, https://doi.org/10.1115/IMECE2017-70165

Zhu, J., Zhu, H., Zhang, J., & Zhang, H. Q. (2019j). A Numerical Study on Flow Patterns inside an Electrical Submersible Pump (ESP) and Comparison with Visualization Experiments. Journal of Petroleum Science and Engineering, 173, 339–350. https://doi.org/10.1016/j.petrol.2018.10.038

Zhu, J., Zhu, H., Cao, G., Zhang, J., Peng, J, Banjar, H., Zhang, H.-Q. (2019k). A New Mechanistic Model To Predict Boosting Pressure of Electrical Submersible Pumps Under High-Viscosity Fluid Flow with Validations by Experimental Data. SPE Journal, SPE-193384 (accepted). https://doi.org/10.2118/194384-PA

APPENDIX A

GLOBAL PARAMETERS AND INITIAL VALUES

The flow conditions and initial guess values used in the simulation by the new model are shown below.

Table A.1: Global parameters and initial values

Parameter	**Initial value**	**Unit**	**Explanation**
π	3.14159	-	pi
g	9.81	m/s^2	Gravitational acceleration
R	8.314	J/mol·K	Constant for ideal gas
M_a	0.02897	kg/mol	Air molecular weight
m_p	5	kg	Plunger mass
L_p	0.4	m	Plunger length
D_p	1.9×0.0254	m	Plunger diameter
C_d	0.1019	-	Plunger falling drag coefficient
A_p	$\pi D_p^2/4$	m^2	Plunger cross-sectional area
H	3048	m	Well depth
D_{ti}	1.995×0.0254	m	Tubing ID
D_{to}	2.125×0.0254	m	Tubing OD
D_a	4.85×0.0254	m	Casing ID
ε	2.5e-4	m	Absolute roughness

A_t	$\pi(D_{to}^2 - D_{ti}^2)/4$	m^2	Tubing cross-sectional area
A_a	$\pi(D_a^2 - D_{to}^2)/4$	m^2	Casing cross-sectional area
P_{res}	5e6	Pa	Reservoir pressure
C_{res}	2.58e-15	-	Reservoir inflow IPR
F_{gout}	0	kg/s	Surface gas mass flow rate
F_{lout}	0	kg/s	Surface liquid mass flow rate
F_{gres}	0	kg/s	Gas flow from reservoir
F_{lres}	0	kg/s	Liquid flow from reservoir
F_{gtub}	0	kg/s	Gas flow into tubing
F_{ltub}	0	kg/s	Liquid flow into tubing
F_{gann}	0	kg/s	Gas flow into annulus
F_{lann}	0	kg/s	Liquid flow into annulus
n	1	-	Reservoir inflow index
GLR	5	kg/kg	Gas liquid ratio
T_{grd}	0.03	K/m	Formation temperature gradient
SG_l	1.06	-	Specific gravity for liquid
SG_g	0.64	-	Specific gravity for gas
M_g	$\gamma_g \cdot M_a$	kg/mol	Gas molecular weight
C_v	0.5e-7	-	Coefficient of motor valve
T_{wh}	288	K	Wellhead temperature
P_c	1.6e6	Pa	Casing pressure
P_{cb}	1.6e6	Pa	Casing bottom pressure

P_t	1.57e6	Pa	Tubing pressure
P_{tb}	1.57e6	Pa	Tubing bottom pressure
P_{pb}	0	Pa	Pressure below plunger
P_{pt}	0	Pa	Pressure above plunger
P_{wf}	0	Pa	Bottom hole pressure
P_l	1.1e6	Pa	Flow line pressure
L_{tt}	5	m	Liquid height on top of plunger
L_{tt0}	5	m	Original liquid height on top of plunger
Ltb	0	m	Liquid height below plunger
La	0	m	Liquid height in annulus
mga	0	kg	Gas mass in annulus
mla	0	kg	Liquid mass in annulus
mgtt	0	kg	Gas mass above plunger
mgtb	0	kg	Gas mass below plunger
mltt	$\rho_l A_t L_{tt}$	kg	Liquid mass above plunger
mltb	0	kg	Liquid mass below plunger
X_p	0	m	Plunger position from well bottom
V_p	0	m/s	Plunger velocity, positive for upward movement
Acc	-1	m/s^2	Plunger acceleration, (- means downward)
t	0	s	Global time
dt	0	s	Time interval

APPENDIX B

CALCULATION FLOW CHART

Figure B.1 shows the calculation flow chart of the new model, where N_{total} is the total plunger lift cycles, t_{cv} is the valve closing time, and T is the period of each plunger lift cycle.

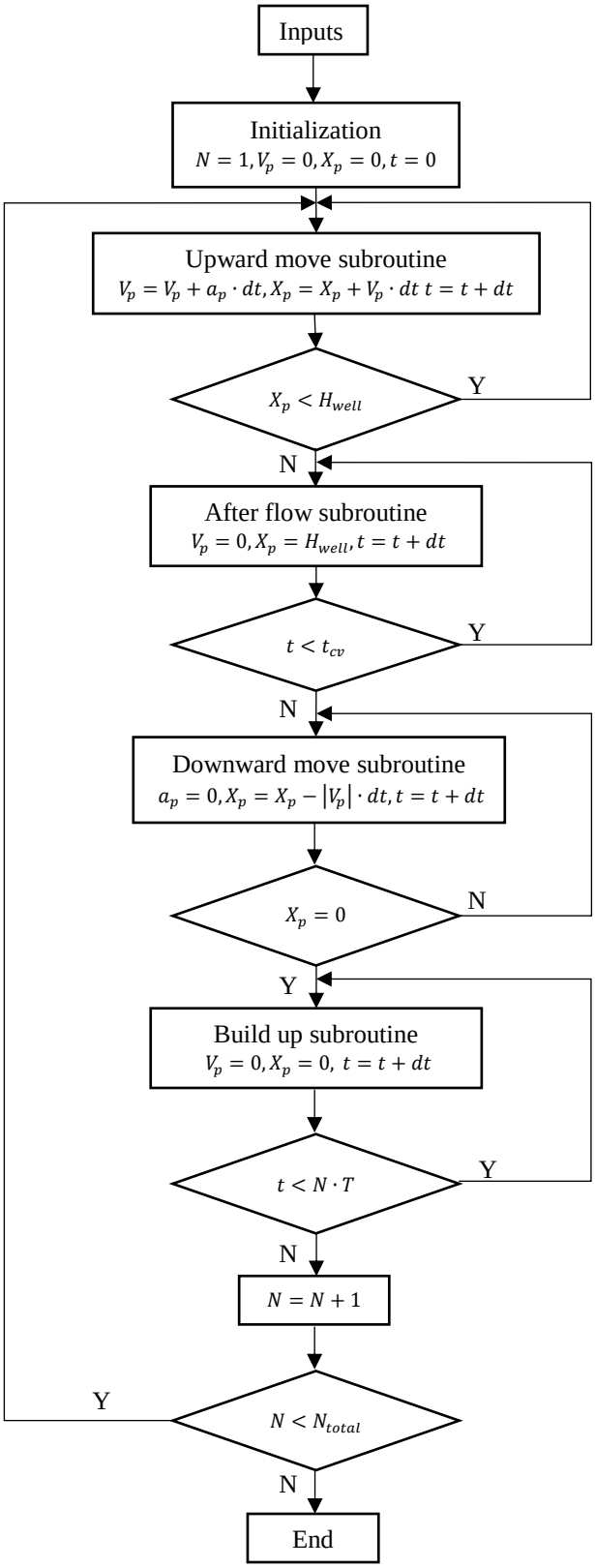

Figure B.1: Flow chart for plunger lift modeling